1   ***Tissue-autonomous immune response regulates stress signalling during hypertrophy.***

2

3   Robert Krautz[1][#][†], Dilan Khalili[1][†], and Ulrich Theopold[1]

4

5   [1]   Department of Molecular Biosciences, The Wenner-Gren Institute (MBW),
6   Stockholm University, Svante Arrhenius väg 20C, 114 18 Stockholm, Sweden
7   [#]   *present address:* The Bioinformatics Centre, Department of Biology,
8   University of Copenhagen, Ole Maaløes Vej 5, 2200 Copenhagen N, Denmark
9   [†]   These authors contributed equally to this work.

10

11 ***Corresponding authors:*** R. Krautz: r.krautz@binf.ku.dk, U. Theopold: uli.theopold@su.se

12

13 ***Abstract***

14

15 Postmitotic tissues are incapable of replacing damaged cells through proliferation, but need to

16 rely on buffering mechanisms to prevent tissue disintegration. By constitutively activating the

17 Ras/MAPK-pathway via *Ras^{V12}*-overexpression in the postmitotic salivary glands of

18 *Drosophila* larvae, we overrode the glands adaptability to growth signals, induced hypertrophy

19 and stress accumulation. This allowed us to decipher a novel, spatio-temporally regulated

20 interaction between the JNK-stress response and a genuine tissue-autonomous immune

21 response. Central to this interaction is the direct inhibition of JNK-signalling by the

22 antimicrobial peptide Drosomycin, which blocks programmed cell death and prevents

23 recognition of the stressed tissue by the systemic immune response. While this mechanism

24 might allow growing salivary glands to cope with temporary stress, continuous expression of

25 Drosomycin favors survival of unrestricted, hypertrophic *Ras^{V12}*-glands. Our findings indicate

26 the necessity for refined therapeutic approaches that fundamentally acknowledge detrimental

27 effects that stimulated immune responses have on tissues coping with damage and stress.

28

29 ***Introduction***

30

31 Immune and stress responses have evolved to protect the organism from both exogenous and

32 endogenous stimuli (Eming, 2014; Adamo, 2017; Rankin and Artis, 2018). By sensing

33 deviations from homeostasis and inducing compensatory mechanisms, immune and stress

34 responses keep physiological parameters within tolerable limits (Hoffmann and Parsons, 1991;

35 Vermeulen and Loeschcke, 2007).

36   Heat shock, radiation, starvation, toxic metabolites, hypoxia or hyperoxia are all well-

37 characterized stressors. They activate stress responses which can ultimately lead to the

38   induction of programmed cell death (Lowe et al., 2004; Loboda et al., 2016). In *Drosophila*,

39   the Keap1-Nrf2-, JNK- and p38-signaling pathways are crucial for mounting these anti-stress-

40   responses (Stronach and Perrimon, 1999; Fuse and Kobayashi, 2017). Immune responses on

41   the other hand, like the Drosophila Toll and Imd pathways, are typically activated by molecular

42   structures exposed on the surfaces of pathogens (Medzhitov and Janeway, 2002; Kurata, 2004).

43   These pathways coordinate the humoral and cellular immune system to eliminate intruding

44   pathogens (Lemaitre and Hoffmann, 2007; Buchon et al., 2014).

45   Humoral immune responses in *Drosophila* are characterized by the production and

46   secretion of large sets of effector molecules, most notably antimicrobial peptides (AMPs) like

47   Drosomycin (Drs) (Imler and Bulet, 2005). AMPs not only target extrinsic threats, but also

48   react to intrinsic stimuli such as tumorigenic transformation with the possibility to induce

49   apoptosis (Araki et al., 2018; Parvy et al., 2019). However, it remains unknown whether AMPs

50   also have functions beyond promoting apoptosis when sensing and reacting to accumulating

51   stress such as during wound healing and tumor formation.

52   Apart from their described individual roles, immune and stress pathways are proposed

53   to be either induced successively or concomitantly dependent on the level of deviation from

54   homeostasis (Chovatiya and Medzhitov, 2014; Ammeux et al., 2016). However, detailed

55   characterisation of wound healing and tumor models in *Drosophila* revealed a more complex

56   picture (Park et al., 2004; Buchon et al., 2009; Meyer et al., 2014; Liu et al., 2015; Wu et al.,

57   2015). Accordingly, immune and stress responses often neither occur separately, nor do they

58   follow a simple linear cascade, but rather regulate each other via context-dependent mutual

59   crosstalk (Liu et al., 2015; Liu et al., 2015; Fogarty et al., 2016; Perez et al., 2017). One

60   recurring motif throughout most of these models is the central role of the stress-responsive

61   JNK-pathway and its frequent interaction with the Toll and Imd immune pathways (Rämet et

62   al., 2002; Galko and Krasnow, 2004; Park et al., 2004; Uhlirova et al., 2005; Igaki et al., 2006;

63   Andersen et al., 2015; Enomoto et al., 2015). However, while JNK-signalling can function

64   either in a tumor-promoting, anti-apoptotic or in a tumor-suppressive, pro-apoptotic manner

65   depending on the context, Toll- and Imd-signalling have only been shown to display a tumor-

66   suppressing, pro-apoptotic role in *Drosophila* (Uhlirova et al., 2005; Igaki et al., 2006; Uhlirova

67   and Bohmann, 2006; Vidal, 2010; Cordero et al., 2010; Enomoto et al., 2015).

68   These tumor-suppressive, pro-apoptotic functions of immune responses have been well

69   characterized and attributed to the secretion of humoral factors or the recruitment of immune

70   cells through the systemic immune system (Babcock et al., 2008; Pastor-Pareja et al., 2008;

71   Hauling et al., 2014; Parisi et al., 2014; Fogarty et al., 2016; Perez et al., 2017). In addition,

72   during clonal cell competition in imaginal discs, Toll- and Imd-signalling were implicated in

73   the elimination of less fit cell clones by inducing apoptosis (Meyer et al., 2014). Importantly,

74   the selective growth disadvantage of these less fit cells is thought to be a response to systemic

75   infection (Germani et al., 2018) and it remains an open question whether genuine tissue-

76   autonomous immune responses can contribute to adaptation of growth during wound healing

77   and tumor formation.

78   The larval salivary gland (SG) of *Drosophila* is a powerful system to study adaptive

79   growth control, since growth is not completely predetermined, but modulated by the nutritional

80   status (Smith and Orr-Weaver, 1991; Britton and Edgar, 1998). In contrast to mitotically active

81   tissues, growth in post-mitotic tissues like the larval SG is based on endoreplication and

82   hypertrophy rather than on cell division (Edgar et al., 2014; Orr-Weaver, 2015). Modifying the

83   underlying, tight growth regulation, for instance by continuous growth signalling via

84   constitutively activated Ras/MAPK-signalling can easily lead to the accumulation of oxidative

85   stress and DNA damage (Mason et al., 2004; Bartkova et al., 2005; Bartkova et al., 2006; Di

86   Micco et al., 2006; Shim et al., 2013; Shim, 2015). However, the parameters defining the natural

87   limit of growth adaptation and the buffering mechanisms in place to cope with prolonged or

88   continuous stress remain poorly understood.

89   Here, we uncover a genuine tissue-autonomous immune response which directly

90   regulates hypertrophic growth and adaptation to accumulating stress in larval SGs. By

91   overexpressing a dominant-active form of the small GTPase Ras, Ras^{V12}, we induced

92   hypertrophic growth. This activates a tissue-autonomous immune response which allows the

93   hypertrophic gland to cope with the resulting stress through spatio-temporally regulated

94   inhibition of the JNK-mediated stress response. We present evidence that tissue-autonomous

95   expression of the AMP Drosomycin (Drs) is at the core of this inhibition: Drs directly interferes

96   with JNK-signalling and inhibits JNK-dependent programmed cell death. This prevents

97   recognition of the stressed tissue by the systemic immune response and allows survival and

98   unrestricted growth of hypertrophic salivary glands.

99

100   ***Results***

101

102   ***Local immune reaction accompanies Ras^{V12}-dependent hypertrophy***

103   In order to identify buffering mechanisms that compensate for continuous stress, we

104   made use of our previously published hypertrophy model in the SGs of *Drosophila* larvae

105   (Hauling et al., 2014). We expressed a dominant-active form of Ras, Ras^{V12}, uniformly across

106 the entire secretory epithelium of SGs throughout larval development by using the Bx^{MS1096}

107 enhancer trap (FigS1A for 96/120 h after egg deposition, AED). To further enhance Ras^{V12}-

108 dependent hypertrophy, we combined Ras^{V12}-expression with RNAi-mediated knockdown of

109 the cell polarity gene *lethal (2) giant larvae* (lgl; FigS1;(Jacob et al., 1987; Strand et al., 1994)).

110 Their individual and cooperative role in tumor formation in mitotic tissues has been well

111 characterized (Bilder et al., 2000; Pagliarini and Xu, 2003; Herranz et al., 2016). Cell- and

112 tissue-morphology was assessed using Phalloidin-rhodamine staining (Fig1A/S1A) and nuclear

113 morphology by DAPI (Fig1B-C/S1B-D).

114 At 96 h AED Ras^{V12}-expressing SG cells retained most of their normal morphology

115 compared to w^{1118}-control glands. However, their integrity and polarity were severely disrupted

116 at 120 h AED (Fig1A/S1A). Nuclei of Ras^{V12}-glands showed a continuous increase in volume

117 at 96 h and 120 h AED (1.33 fold compared to w^{1118} controls at 96 h AED; 5.66 fold at 120 h

118 AED; Fig1C) and signs of nuclear disintegration at 120 h AED implying the induction of

119 programmed cell death (PCD; Fig1B). Both loss of cell integrity and nuclear disintegration

120 coincided temporarily (Fig1A-B), and were exacerbated upon coexpression of lgl^{RNAi} (FigS1A-

121 D). These results confirm our previous findings and demonstrate that continuous growth

122 signalling in larval salivary glands leads to increased organ size accompanied with additional

123 endocycles at 96 h AED, both hallmarks of compensatory hypertrophy (Hauling et al., 2014:

124 Tamori and Deng, 2014). Furthermore, the additional, Ras^{V12}-induced endoreplications without

125 obvious effect on tissue integrity imply an adaptability to excess growth signalling, whereas the

126 subsequent collapse of nuclear integrity and cellular polarity at 120 h AED delineate its

127 limitations.

128 To characterize the mechanisms involved in the early phase of SG growth adaptation at

129 96 h AED, we performed total RNA sequencing of complete Ras^{V12}-expressing and w^{1118}-

130 control SGs dissected at 96 h AED prior to cellular and nuclear disintegration. The most

131 significantly upregulated gene in Ras^{V12}-glands compared to their w^{1118}-counterpart was

132 Ras85D itself (q-value=$6.51 \cdot 10^{-282}$), which validates the experimental set-up (Fig1D). The most

133 differentially expressed gene was the AMP Drs, which indicates the activation of a local

134 immune response in Ras^{V12}-glands. To evaluate this further, we employed a GFP reporter for

135 Drs and observed strong induction in Ras^{V12}-glands, but not in any other larval tissue

136 (Fig1E/S1E; Ferrandon et al., 1998a). At 96 h AED the entire secretory epithelium of the SG

137 expressed Drs with a strong tendency for increased induction in the proximal part (PP) closest

138 to the duct (Fig1E). At 120 h AED Drs was almost exclusively expressed in the PP (Fig1E/S1E).

139 In order to assess whether immune cells were recruited as part of a parallel systemic response,

140   we stained glands with an antibody against the pan-hemocyte-marker Hemese. While Ras^{V12}-
141   glands were completely devoid of hemocytes at 96 h AED, at 120 h AED they were recruited
142   to the gland surface. However, hemocyte attachment was restricted to the distal, non-Drs
143   expressing part (DP), rendering Drs expression and hemocyte attachment across the gland
144   epithelium mutually exclusive (Fig1E-F). Coexpression of lgl^{RNAi} elevated the level of recruited
145   hemocytes at 120 h AED and pre-empted this recruitment to the DP already at 96 h AED
146   (FigS1E-F).

147   We next investigated whether the change in nuclear volume as a marker for growth
148   adaptation follows a similar proximal-distal-divide as Drs-expression and hemocyte attachment
149   (FigS1C). Nuclei in the DP of the SG at 96 h AED showed a moderate volume increase upon
150   Ras^{V12}-expression compared to distal w^{1118}-control nuclei. However, after 120 h AED distal
151   nuclei had undergone a drastic increase in nuclear volume (6.28 fold compared to distal w^{1118}-
152   control nuclei) while nuclei in the proximal part of the SG displayed only a moderate increase
153   in size compared to w^{1118}-control nuclei, that did not increase over time. This indicates that
154   nuclei in the DP of Ras^{V12}-glands undergo more rounds of endoreplication than their proximal
155   counterparts coinciding with the decline of Drs-expression and an increase in hemocyte
156   attachment in this part.

157

Dorsal-dependent Drs expression is part of a genuine tissue-autonomous immune response

159   As barrier epithelia, the lumen of the SG forms part of a continuum with the exterior,
160   exposing them to extrinsic stimuli including nutritional cues and pathogens (Andrew et al.,
161   2000). Since systemic infection can modulate tissue growth, we sought to clarify whether the
162   observed local immune response in the gland epithelium fulfills the criteria of a genuine tissue-
163   autonomous immune response or was rather embedded in a wider systemic immune response
164   (Germani et al., 2018). Therefore, we eradicated any influence by putative systemic infections,
165   food-derived signals and pathogens or bacterial contamination by raising larvae with Ras^{V12}-
166   glands under axenic conditions, on minimal medium or by bleaching embryos (FigS2A'-A''';
167   Smith and Orr-Weaver, 1991; Britton and Edgar, 1998; Ryu et al., 2008; Piper et al., 2014).
168   None of these changes diminished the Drs expression, strongly indicating that Drs is indeed
169   induced in a *bona fide* tissue-autonomous manner as a response to Ras^{V12}-dependent
170   hypertrophic growth (FigS2A'-A'''; Colombani et al., 2005; Mirth et al., 2014).

171   We further sought to identify the upstream factors controlling Drs expression. The
172   homeobox-like transcription factor Caudal is necessary for Drs expression in the female
173   reproductive organs and the adult SG (Ferrandon et al., 1998a; Han et al., 2004; Ryu et al.,

174   2004). However, RNAi-lines directed against Caudal or its canonical interaction partner,

175   Drifter/vvl, did not reduce Drs-expression in Ras^{V12}-glands indicating that the regulation of Drs

176   expression as part of the tissue-autonomous immune response is clearly different from its

177   counterpart in the adult SG (FigS2B; Junell et al., 2010).

178   In order to evaluate whether either Toll- or - as is the case for local infections - Imd-

179   signalling plays a role in Drs expression, we used the reproducible fluorescence pattern of the

180   Drs-GFP reporter at 96 h AED to assay RNAi-lines directed against canonical components of

181   both pathways in Ras^{V12}-glands (Fig2A; see 'Materials and methods' for scored phenotypes;

182   Ferrandon et al., 1998a; Tzou et al., 2000; Takehana et al., 2004; Wagner et al., 2009). Of the

183   11 RNAi-lines tested, only one targeting the NFκB-transcription factor Dorsal significantly

184   reduced the fluorescence signal of the Drs-reporter (Fig2A). However, Drs expression is

185   completely independent of the upstream modules of the two classical Drosophila immune

186   pathways, Toll and Imd.

187   At 96 h AED Dorsal was present in the entire secretory epithelium of both Ras^{V12}- and

188   w^{1118}-control glands. In contrast, at 120 h AED its expression was confined solely to the PP

189   (Fig2B). This overlapped with the Drs-mRNA expression as determined by in situ hybridization

190   (ISH; Fig2SC). Furthermore, both SG-specific knock-down or whole organism homozygous

191   knock-out (dl[15]) of Dorsal completely abolished Drs-expression in the DP of the gland at 96 h

192   AED and drastically reduced it in the proximal part at both time points in line with our results

193   from the reporter assay (Fig2A-B/S2D).

194   Together, our results indicate that the spatio-temporal dynamics of Drs expression are a

195   consequence of the decrease in endogenous Dorsal expression, independent of canonical Toll-

196   and Imd-signalling. While regulation of Dorsal expression is Ras^{V12}-independent, Drs is only

197   expressed in the presence of Dorsal during Ras^{V12}-induced hypertrophy (FigS2E).

198

199   ***Hypertrophy in SGs induces parallel immune and stress responses***

200   Between 96 h and 120 h AED, the decrease in Drs-expression (Fig1E; Fig2B-C) is

201   correlated with deterioration of tissue integrity (Fig1A-B) in the DP of hypertrophic Ras^{V12}-

202   glands. Thus, we hypothesized that the tissue-autonomous immune response and Drs-

203   expression aid in preventing the collapse of nuclear as well as cellular integrity until 96 h AED

204   in the DP and until 120h AED in the PP.

205   To identify possible targets and effector mechanisms of the immune response that buffer

206   the detrimental effects of hypertrophic growth, we analysed the transcriptome data acquired for

207   the w^{1118}-control and Ras^{V12}-glands at 96 h AED in further detail. In order to distinguish whether

208   the differences between Ras^{V12}- and $lgl^{RNAi};Ras^{V12}$-glands (FigS1B-F) are of quantitative or

209   qualitative nature and to characterize the PP with its persistent Dorsal and Drs expression in

210   depth, we also profiled transcriptomes of entire $lgl^{RNAi};Ras^{V12}$-glands and solely the proximal

211   part of $lgl^{RNAi};Ras^{V12}$-glands at 96 h AED (FigS3A; see 'Materials and methods').

212   The sets of significant and differentially upregulated genes (i.e., $log2(beta){\geq}1$; q-

213    $value{\leq}0.05$) for all three conditions (i.e., Ras^{V12} / $lgl^{RNAi};Ras^{V12}$ / $lgl^{RNAi};Ras^{V12}$-PP each

214   normalized to w^{1118}-controls) were intersected to determine common and specific genesets

215   (Fig3A). Notably, the two biggest genesets are differentially upregulated genes shared between

216   all three conditions and genes specifically upregulated in the PP (Fig3A). Furthermore, while

217   all 6 Ras^{V12}- and $lgl^{RNAi};Ras^{V12}$-replicates are in close proximity along the first two principle

218   components in the PCA, the sets of replicates for w^{1118} and especially the PP are very distant

219   from the rest emphasizing the distinctiveness of the PP compared to the rest of the gland (Fig3B).

220   By screening for enriched gene ontology (GO) terms amongst the significantly

221   upregulated genes in the PP of $lgl^{RNAi};Ras^{V12}$-glands in comparison to the entire w^{1118}-glands,

222   we identified genes belonging to the GO-term 'immune response' (i.e., GO:0006955) as

223   significantly enriched (Fig3C; p-value=$1.45{\cdot}10^{-4}$). Detailed examination of the fold-enrichment

224   of these genes across all three experimental groups (i.e., Ras^{V12} / $lgl^{RNAi};Ras^{V12}$ / $lgl^{RNAi};Ras^{V12}$-

225   PP) showed a preferential expression in the PP, too (17 of 30 genes highest expressed in PP;

226   blue arrowheads in Fig3C). In addition, 5 of the top 20 upregulated genes in the PP belong to

227   this GO-term as well. Thus, the Drs-expression we observed using reporter lines serves as a

228   proxy for a more complex, tissue-autonomous immune response in hypertrophic glands,

229   especially in the PP. Nonetheless, Drs itself remains one of the top significantly, differentially

230   upregulated genes across all three conditions (Fig1D; FigS3C; not shown for $lgl^{RNAi};Ras^{V12}$). In

231   fact, Drs-expression in the PP compared to the two conditions for entire glands is even further

232   increased, confirming the strong tendency for proximal over distal Drs-GFP reporter activation

233   (Fig1E; Fig2B).

234   A similar GO-term analysis amongst significantly, upregulated genes in entire Ras^{V12}-

235   or $lgl^{RNAi};Ras^{V12}$-glands revealed the enrichment of genes associated with GO-terms related to

236   'growth', 'salivary gland development' and 'EGFR signalling' consistent with the studied

237   tissue and the induced Ras^{V12}-overexpression. In addition, the lack of unique, significantly

238   enriched GO terms and thus distinct gene expression signatures for either Ras^{V12}- or

239    $lgl^{RNAi};Ras^{V12}$-glands at 96 h AED excludes qualitative differences between these two

240   genotypes as an explanation for their phenotypic differences (FigS1).

241   Importantly, we detected signatures of an activated JNK-cascade as well as cell death

242   in Ras^{V12}- and $lgl^{RNAi};Ras^{V12}$-transcriptomes indicating the presence of an activated stress

243   response and confirming the stimulation of PCD as implied by nuclear disintegration at 120 h

244   AED (Fig1B;Fig3D/S3B GO:0006955; GO:0008219). To validate these signatures further, we

245   performed qPCR for canonical JNK-targets at 96 h AED and found that the expression of all

246   tested genes was significantly increased compared to w^{1118}-control glands (Fig3E/S3C). We

247   used the TRE-GFP1b-reporter construct, which recapitulates JNK-activation by expressing

248   GFP under the control of binding sites for JNK-specific AP-1 transcription factors (Fig3E;

249   Chatterjee and Bohmann, 2012). This not only confirmed JNK-signalling in Ras^{V12}-glands, but

250   also uncovered its prevalence in the DP of these glands at 96 h and 120 h AED consistent with

251   the transcriptome data (Fig3E/S3C). Moreover, the elevated fluorescence signal in the DP at

252   120 h AED compared to 96 h AED implies an increase in activation over time correlating with

253   the collapse of nuclear and cellular integrity during this period (Fig3E/S3C).

254   In summary, the transcriptome analysis confirms our findings that Ras^{V12}-

255   overexpression induces a strong tissue-autonomous immune response in the PP of the SG,

256   beyond sole Drs expression. In contrast, the DP shows a striking increase in JNK-signalling

257   which correlates with decreasing Drs expression and cellular and nuclear disintegration at 120

258   h AED, consistent with the described role of JNK target genes in PCD.

259

Drs overexpression and JNK inhibition prevent Ras^{V12}-induced tissue disintegration

261   The increase in JNK-signalling in the DP of the SG as revealed by our transcriptome

262   analysis coincided in space and time with the downregulation of Drs suggesting an interaction

263   between the tissue-autonomous immune response and the stress response.

264   To test this assumption, we first overexpressed either Drs or a dominant negative form

265   of the *Drosophila* Jun kinase basket individually with Ras^{V12} throughout the entire secretory

266   epithelium of the SG (Fig4A). Either Drs overexpression or JNK inhibition had a profound

267   effect on the gland size, which was significantly increased at 120 h AED, compared to Ras^{V12}

268   only (Fig4B/S4A).

269   Importantly, despite this size increase, glands of both genotypes (i.e., Drs,Ras^{V12} /

270     $bsk^{DN};;Ras^{V12}$) showed no morphological abnormalities and resembled control w^{1118}- much

271   more than Ras^{V12}-glands (Fig4A-B). Strikingly, $bsk^{DN};;Ras^{V12}$- and Drs,Ras^{V12}-glands were

272   completely devoid of attached hemocytes (Fig4B-C). Given the basement membrane's (BM)

273   role in directly regulating organ morphology, the rescue of the gland shape upon coexpression

274   of either Drs or bsk^{DN} with Ras^{V12} pointed towards changes in the integrity of the BM (Ramos-

275   Lewis and Page-McCaw, 2019). In addition, previous reports suggested that hemocytes are only

276   recruited to tissue surfaces upon tissue disintegration and when the integrity of the BM is lost

277   (Kim and Choe, 2014). Hence, to trace the BM we used an endogenous GFP-trap in the *viking*

278   gene, which encodes one subunit of CollagenIV (Fig4B-C). Both in the presence of Drs or by

279   inhibiting basket, the BM remained a continuous sheet surrounding the entire gland, whereas

280   the BM on the surface of Ras^{V12}-glands was clearly disrupted.

281   Matrix metalloproteinases (MMPs) are likely candidates for executing the disruption of

282   the BM and known target genes of the JNK-pathway (Hauling et al., 2014; Stevens and Page-

283   McCaw, 2012; Uhlirova and Bohmann, 2006). In order to see whether hypertrophic glands

284   express MMPs, we performed qPCR for MMP1 and MMP2 at 96 h and 120 h AED on Ras^{V12}-

285   and control w^{1118}-glands. At 96 h AED, Ras^{V12}-glands already exhibit increased MMP1

286   expression (Fig4C-D). However, MMP2 only reaches a significant level of expression at 120 h

287   AED coinciding with the appearance of hemocyte attachment (Fig4D). SG-wide, Ras^{V12}-

288   independent overexpression of MMP2, but not of MMP1, caused opening of the BM and

289   hemocyte attachment to the surface (Jia et al., 2014). This indicates the necessity for a JNK-

290   dependent expression of MMP2 in the hypertrophic Ras^{V12}-glands prior to the recruitment of

291   hemocytes to the tissue surface (Fig4E/S4B).

292   Taken together, overexpression of Drs alone is sufficient to mimic the inhibition of the

293   JNK-pathway in Ras^{V12}-glands: both lead to excess hypertrophic growth compared to Ras^{V12}-

294   glands, but simultaneously prevent tissue disintegration and PCD. Prohibiting the disruption of

295   the basal membrane inhibits hemocyte recruitment and thus prevents the systemic immune

296   response from sensing hypertrophic growth. This in turn suggests that the endogenous Drs

297   expression in Ras^{V12}-glands is seminal for maintaining nuclear and tissue integrity and thus part

298   of the buffer mechanism to adapt to continuous growth signalling.

299

300   ***Drs inhibits JNK-signalling***

301   The strong correlation between loss of Drs and the increase in JNK-signalling in the DP

302   of Ras^{V12}-glands between 96 h and 120 h AED indicated an active interaction between Drs and

303   the JNK-pathway, which prompted us to resolve their hierarchy by epistatic analysis.

304   Coexpression of bsk^{DN} with Ras^{V12} did not deplete Drs in the proximal part of 120 h-old

305   glands, since neither the fluorescence signal of the Drs-GFP reporter nor staining for

306   endogenous *Drs*-mRNA via ISH showed any effects, which excludes a direct regulation of Drs

307   by JNK-signalling (Fig4A;FigS5A). qPCR for Drs in Ras^{V12}- and bsk^{DN};Ras^{V12}-glands

308   confirmed these results further (FigS5B). In contrast, qPCR in hypertrophic Ras^{V12}-glands

309   showed a significant reduction in expression of JNK target genes upon coexpression of Drs at

310   96 h and 120 h AED (Fig5B/S5C-D), in line with a decrease in activated basket (Fig5C,E) and

311   TRE-GFP1b signal in *Drs,Ras^{V12}*- compared to *Ras^{V12}*-glands (Fig5B,D,F). Thus, the

312   overexpression of the AMP Drs actively and tissue-autonomously inhibits the JNK-dependent

313   stress response in hypertrophic *Ras^{V12}*-glands beyond 96 h AED.

314   In addition, we used an efficient RNAi-line against Drs, which in combination with

315   Ras^{V12} reduced Drs-expression drastically compared to its expression in *Ras^{V12}*-glands

316   (FigS5C-D). All significantly upregulated JNK-target genes in *Ras^{V12}*-glands apart from *upd2*

317   were further increased upon knockdown of Drs at 96 h AED (FigS5C). However, this effect

318   ceased at 120 h AED consistent with the canonical loss of Drs expression in the DP of *Ras^{V12}*-

319   glands (Fig5D). This result demonstrates that until 96 h AED the endogenously expressed Drs

320   has the same inhibitory effect on the JNK-pathway as the Drs-overexpression has at 120 h AED.

321

322   ### *Drs prevents cell death in Ras^{V12}-glands*

323   The capacity to induce apoptosis is a well-established function of the JNK-pathway in

324   *Drosophila* (Uhlirova et al., 2005; Igaki et al., 2006; Uhlirova and Bohmann, 2006; Cordero et

325   al., 2010; Enomoto et al., 2015). Combined with the identification of 'cell death' as a

326   significantly enriched term in the GO-analysis, we hypothesized that the observed nuclear

327   disintegration in *Ras^{V12}*-glands after 96 h AED was a consequence of the JNK-dependent

328   induction of PCD (Fig1B-C/S1B-D; Fig3D/S3B).

329   In mitotic tissues, the apoptotic inducer *head involution defective* (hid) is inhibited by

330   Ras/MAPK-signalling (Bergmann et al., 1998; Kurada and White, 1998). However, in *Ras^{V12}*-

331   glands hid expression gradually increased from 96 h to 120 h AED coinciding with the increase

332   in nuclear disintegration (Fig6A). Coexpression of Drs with *Ras^{V12}* significantly decreased hid

333   expression at both time points, while Drs knock-down in *Ras^{V12}*-glands increased hid

334   expression even further already at 96 h AED. Together with the reduction in hid expression

335   upon JNK-inhibition in *bsk^{DN};;Ras^{V12}*-glands, Drs emerges as a negative regulator of the

336   apoptotic inducer hid by inhibiting JNK-signalling (FigS5B).

337   To evaluate the induction of PCD in *Ras^{V12}*-glands, we either inhibited JNK-signalling

338   at the level of basket activation or coexpressed the caspase-inhibitor p35 with *Ras^{V12}* and

339   examined nuclear volume and integrity (Fig6B-D). p35 inhibits Drice and thus blocks PCD at

340   the level of effector caspase activation (Hawkins et al., 2000; Hay et al., 1994; Meier et al.,

341   2000). While both interventions successfully blocked nuclear disintegration, the additional

342   rounds of endoreplication as observed in *Ras^{V12}*-glands were not suppressed (Fig6C-D).

343 Crucially, Drs-coexpression in Ras^{V12}-glands phenocopies the inhibition of JNK-signalling and

344 effector caspases both in terms of restoring nuclear integrity as well as the persistence of excess

345 endoreplications.

346 Last, to validate the inhibition of PCD by Drs, we monitored Dronc activity using the

347 cleaved caspase 3 antibody (CC3). In fact, the strongest Dronc activity occurred in cells that

348 also displayed heavy disintegration of nuclei, confirming the relation between caspase

349 activation and nuclear disintegration as part of PCD (FigS6A-B). However, in Drs,Ras^{V12}-

350 glands Dronc was significantly less activated compared to Ras^{V12}-glands (Fig6E-F; Fan and

351 Bergmann, 2010).

352 Taken together, we show that JNK-dependent induction of PCD is a consequence of the

353 collapse in adaptation to Ras^{V12}-induced hypertrophy. Importantly, overexpression of Drs in

354 Ras^{V12}-glands prevents PCD by blocking full JNK-activation. This is in contrast to recent

355 observations where AMPs, including Drs, act pro-apoptically aiding in the elimination of tumor

356 cells and limiting tumor size (Araki et al., 2018; Parvy et al., 2019).

357

Drs inhibits the JNK-feedback loop

359 Various *Drosophila* models for tissue transformation have shed light on the functional

360 separation of the JNK-pathway into an upstream kinase cascade leading to basket-activation

361 and a downstream feedback-loop converging again on basket activation (Fig7A; Shlevkov and

362 Morata, 2012; Fogarty et al., 2016; Muzzopappa et al., 2017; Perez et al., 2017).

363 Our results revealed a negative regulatory impact of Drs on JNK-signaling in Ras^{V12}-

364 glands, but did not determine which part of the pathway is targeted by Drs. To answer this

365 question, we uncoupled the feedback loop from the upstream kinase cascade by solely

366 overexpressing hid (Fig7A). Irrespective of the differing models for the signal propagation

367 downstream of Dronc, this initiator caspase remains seminal for establishing the actual

368 feedback with basket (Shlevkov and Morata, 2012; Fogarty et al., 2016). Thus, we stained

369 glands for activated Dronc and basket after a pulse of hid-overexpression during the larval

370 wandering stage (Fig7A). As expected, *hid*-expressing glands showed highly elevated levels of

371 activated Dronc, but also basket, which indicates the presence of feedback activation. Moreover,

372 both phenotypes were reversed upon coexpression of Drs during the hid-expression pulse

373 (Fig7B-C,E). Thus, Drs seems to inhibit JNK-signalling downstream of hid and upstream of

374 Dronc and basket, emphasizing an inhibition of the JNK-feedback loop rather than the initial

375 kinase cascade.

376   To clarify that Drs operates in a similar fashion during Ras^{V12}-induced hypertrophic

377   growth, we stained Ras^{V12}-glands (Fig6E-F) for activated basket in the presence and upon

378   knock-down of Dronc (Fig7D,F/S7A-B). In fact, the absence of a signal for activated basket in

379    $Dronc^{RNAi};Ras^{V12}$- compared to strong Ras^{V12}-glands confirms the presence of a genuine

380   feedback-regulation as part of JNK-signalling in SGs.

381

382   ***Discussion***

383

384   ***Tissue-autonomous vs. systemic immune response mediated via JNK-signalling***

385   By overexpressing Ras^{V12} in larval SGs, we made use of and overrode the gland's ability

386   to adapt to growth signals. Activating constitutive Ras/MAPK-signalling allowed us to identify

387   local immune and stress responses as part of a buffering mechanisms to compensate the

388   accumulation of stress and decipher natural limits of growth adaptation (Hauling et al., 2014).

389   Remarkably, in this context the local immune response inhibits the parallel stress response, an

390   effect that to our knowledge has not been described before. Central to this inhibition is the AMP

391   Drs, which directly impinges on the JNK-pathway and thereby subsequently also on inducing

392   apoptosis, a function completely opposite to previous observations in other tissues (Araki et al.,

393   2018; Parvy et al., 2019). These results also indicate an unprecedented role for an AMP as a

394   signal transducer enabling tissue-autonomous crosstalk between immune and stress pathways.

395   Dependent on the extent of JNK-inhibition by the local, Drs-dependent immune response and

396   thus the integrated decision of both on the state of the tissue's homeostasis, the gland epithelium

397   attracts hemocytes as part of a wider, systemic immune response. By virtue of inhibiting JNK-

398   signalling, tissue-autonomous and systemic immune response antagonize each other, a balance

399   that decides on continuos hypertrophic growth or its restriction (Fig8). The latter has far

400   reaching implications for therapeutic approaches that need to consider the adverse effects that

401   stimulating immune responses might have on tissue growth after damage and under stress.

402

403   ***Drs is expressed as part of a genuine tissue-autonomous immune response***

404   The salivary glands of *Drosophila* larvae are an integral part of its gastrointestinal

405   system and the lumen of the mature glands forms a continuum with the exterior. As such the

406   glands are constantly exposed to microbial and pathogenic influences, which predestines them

407   to be a dedicated immunological barrier epithelium. However, raising larvae with Ras^{V12}-glands

408   under strictly axenic conditions corroborated the authenticity of the immune response as truly

409   tissue-autonomous and thus independent of exogenous or systemically distributed pathogenic

410 stimuli. This is further emphasized by the dependency of Drs expression on the tissue-specific

411 overexpression on Ras^{V12} and tissue-autonomous manipulations (i.e., Drs or bsk^{DN}

412 overexpression) leading to the inhibition of JNK-activation and hemocyte recruitment.

413 However, apart from Dorsal neither the homeobox transcription factor Caudal as in the

414 adult glands nor any other of the canonical members belonging to the Toll- and Imd-pathway

415 are involved in Drs expression (Ferrandon et al., 1998b; Hauling et al., 2014; Ryu et al., 2004).

416 Under wild-type conditions, Dorsal is expressed throughout the entire gland epithelium until

417 96 h AED, but only remains expressed in the PP at 120 h AED (Fig2B). This spatio-temporal

418 expression pattern in turn determines the expression of Drs in Ras^{V12}-glands essentially

419 separating the gland at 120 h AED into an immunocompetent duct-proximal and a stress-

420 responsive duct-distal compartment (Fig2B,Fig8). Due to the absence of Drs in the DP at 120

421 h AED, stress-responsive JNK-signalling finally exceeds a critical threshold leading to elevated

422 MMP2- and hid-expression. This stimulates the onset of PCD and opening of the basal

423 membrane as a prerequisite for attachment of hemocytes that are subsequently recruited to the

424 surface of the SGs (FigS2E,Fig8; Hauling et al., 2014). To the contrary, Dorsal continues to

425 induce Drs in the PP of Ras^{V12}-glands until 120 h AED in line with the complete absence of

426 hemocyte recruitment to this part of the gland (Fig1F/S1B-C).

427

Drosomycin impinges on JNK feed-back activation

429 In depth analysis of wound regeneration and tumor formation has shed light on the

430 intricate architecture of the JNK-pathway and its signal propagation (Santabarbara-Ruiz et al.,

431 2015; Pinal et al., 2018). This has led to the discovery of feedback- or self-sustenance-loops as

432 part of JNK-signalling (Shlevkov and Morata, 2012; Fogarty et al., 2016; Muzzopappa et al.,

433 2017; Perez et al., 2017). Similarly, several lines of evidence validated the existence of a

434 complex quantitatively and qualitatively regulated activation of the JNK-pathway in Ras^{V12}-

435 glands. In fact, the strong reduction of basket activation upon knock-down of the initiator

436 caspase Dronc in the Ras^{V12}-background at 120 h AED indicates that a feedforward-loop is also

437 part of the propagation of JNK-activation in hypertrophic glands (Fig7D,F/S7A-B).

438 Consistently, even sole hid overexpression in SGs led to Dronc as well as basket activation

439 emphasizing the presence of this feedback-regulation as part of the JNK-pathway further

440 (Fig7B-C,E).

441 In general, feedback loops serve as a predestined platform to integrate additional signals

442 via crosstalk with other pathways to dynamically modulate the originally, transmitted signal

443 and thus either amplify or weaken the response (Antebi et al., 2017; Kholodenko, 2006). Here,

444   we describe a novel mode of signal attenuation by the tissue-autonomous immune response that

445   rather than eliminating an exogenous stimulus directly interferes with the signal propagation in

446   the JNK-feedback loop. Fundamentally, this interaction is part of an emerging picture of

447   crosstalk between immune and stress responses involved in organ growth and maintenance in

448   *Drosophila* (Hauling et al., 2014; Liu et al., 2015; Parisi et al., 2014; Wu et al., 2015).

449   Drs regulates the signal propagation of the intracellular module of the JNK-pathway

450   and throughout our experiments only directly Drs expressing cells prevented Ras^{V12}-induced

451   cell disintegration and PCD. However, it remains an outstanding question whether Drs

452   functions exclusively cell-autonomously and intracellularly or whether secreted Drs operates

453   in an autocrine manner too. Clonal analysis and rescue experiments will serve this purpose in

454   the future. Further work on the effector mechanism of Drs will also elucidate further details

455   about the components of the JNK-feedback loop in- or directly regulated by Drs. This will also

456   contribute to mapping the manifold modes of immune-stress-crosstalk in *Drosophila* and find

457   general patterns among them beyond a sole dependency on the specific context.

458

459   ***Drs promotes hypertrophic growth and inhibits PCD***

460   As our *Drs,Ras^{V12}*-experiments indicated, under conditions of continuous growth and

461   therefore chronic stress induction, the ability to suppress the JNK-pathway in a Drs-dependent

462   manner supports continuous, hypertrophic growth of Ras^{V12}-glands and the survival of the

463   tissue. Moreover, a prolongation of Drs-expression beyond its endogenous decrease inhibits the

464   induction of PCD and the recognition of the systemic immune response and thus renders the

465   hypertrophic gland unchallenged.

466   In fact, while Ras/MAPK-signalling in mitotic tissues crucially suppresses apoptosis by

467   downregulating hid expression, this effect is revoked in hypertrophic Ras^{V12}-glands (Bergmann

468   et al., 1998; Kurada and White, 1998). While the reason for this difference remains to be

469   elucidated, it is in fact Drs which operates as the inhibitor of apoptotic inducers in hypertrophic

470   glands. This function is central to the suppression of PCD in Ras^{V12}-glands (Fig6A).

471   This differs fundamentally from the pro-apoptotic function of AMPs, which was recently

472   described for two tumor models. In both disc (discs large, *dlg,* Parvy et al., 2019) and leukemic

473   tumors (mxc[mbn1], Araki et al., 2018), AMPs were shown to target tumor cells and limit tumor

474   size by inducing apoptosis. In addition to the differences between the tumorous tissues (i.e.,

475   proliferative discs and lymph glands), the fact that Drs is induced locally in SGs and acts tissue-

476   autonomously may explain its different activities.

477

478 ***Hypertrophic SGs are a remarkable system to discover buffer mechanisms***

479   Being incapable of cell proliferation, damaged postmitotic tissues can't rely on

480   regenerative cell plasticity like imaginal discs or stem cell-derived tissue regeneration as in the

481   *Drosophila* adult midgut (Ohlstein and Spradling, 2006; Herrera et al., 2013; Herrera and

482   Morata, 2014; Schuster and Smith-Bolton, 2015; Ahmed-de-Prado and Baonza, 2018). Instead,

483   they need to cope with endogenous and exogenous influences via elaborate mechanisms to

484   prevent or buffer detrimental consequences.

485   Here, we show that continued Ras^{V12}-expression in the larval salivary gland overrides

486   the dependency on nutritional cues and stimulates excess endoreplications that eventually have

487   damaging effect on the tissue integrity by inducing elevated levels of stress. Uninterrupted

488   induction of endoreplications has its natural limits in every system, even in salivary glands that

489   are already polyploid. Eventually, continuous induction of more endocycles is challenged by

490   nutritional restrictions in synthesizing more DNA, replication stress, spatial limitations in the

491   gland nuclei and continuously more unsynchronized metabolic turnover. Hence, in spite of the

492   anti-apoptotic function Ras^{V12} conveys in mitotic tissues, unrestricted stimulation of excess

493   endoreplications ultimately leads to cell death. Since this characterizes the final collapse of

494   tissue homeostasis, it also allows to study the extent of buffering capacity conveyed by immune

495   and stress-responsive signalling.

496   Thus, hypertrophic Ras^{V12}-glands constitute an outstanding system to study the

497   involvement of tissue-autonomous immune and stress-induced responses to buffer deviation

498   from homeostasis.

499

500 ***Immune surveillance theory***

501   According to the immune surveillance theory, the immune system has evolved to reduce

502   the risk of somatic cells accumulating cancerous mutations (Burnet, 1970; Burnet, 1957). In

503   order to reduce the danger of cell-transformation, cells express or expose molecules upon

504   recognition of stress or damage during transformation. These markers are sensed by the immune

505   system, which in turn eradicates the potentially harmful cells. (Jung et al., 2012; Vantourout et

506   al., 2014; Schmiedel and Mandelboim, 2018). However, the immune surveillance theory

507   remains controversial, since tumor-associated inflammation was also shown to promote rather

508   than suppress tumor growth (Balkwill and Mantovani, 2001; Mantovani et al., 2008). Our

509   model bridges the gap between these two opposing views, since the effects of the tissue-

510   autonomous and systemic immune responses appear to be antagonistic regarding the regulation

511   of JNK-activation and thus ultimately PCD. In fact, only the integration of the various stress

512 and immune mechanisms in hypertrophic Ras^{V12}-glands allows a concerted decision to
513 eradicate a putatively dangerous cell via inducing PCD or not. Given the evolutionary
514 conservation from insects to mammals of signalling pathways that govern growth control
515 (Edgar, 2006), it is likely that mechanisms to detect and counteract a loss in regulation of these
516 pathways, such as stress and immune pathways, are similarly conserved between both phyla.

517

518 ***Material and methods***

519

520 ***Fly husbandry and stocks***

521 All crosses were reared on standard potatomash/molasses medium under tempered conditions (see
522 'Staging') in a 12h dark/12 h light-cycle. Drs-GFP (W.-J. Lee), UAS-dfr^{RNAi} (S.Certel), TRE-GFP1b (D. Bohmann),
523 UAS-Drs (B. Lemaitre), dl^{15} (Y. Engström), UAS-hid (M.Suzanne), UAS-MMP2$^{\#4}$, UAS-MMP1^{APM1037} and UAS-
524 MMP1^{APM3099} (A. Page-McCaw) were kind gifts from the indicated donors. The generation of the CollagenIV
525 flytrap line vkg^{G00454} was described in (Morin et al., 2001). Please, see supplementary file 1 for complete list of
526 experimental crosses.

527

528 ***Staging***

529 Virgins were collected for 3-7 d before setting crosses. Initially, crosses were kept on standard food
530 without antibiotics for 48 h at 25°C. Eggs were collected for 6 h (Immunohistochemistry and qPCR) or for 2 h
531 (RNASeq) at 25°C. When necessary, precollections were performed for 2 h at 25°C prior to the actual collection.
532 Egg collections were incubated for 24 h at 29°C or for hid experiments 48 h at 18°C and batches of 24 hatched 1st
533 instar larvae were afterwards transferred to vials with 3 ml standard food supplemented with Neomycin (0.1
534 mg·ml^{-1}, Sigma-Aldrich, N1876), Vancomycin (0.1 mg·ml^{-1}, Sigma-Aldrich, V2002), Metronidazol (0.1 mg·ml^{-1},
535 Sigma-Aldrich, M3761) and Carbenicillin (0.1 mg·ml^{-1}, Sigma-Aldrich, C1389). After incubation at 29°C for
536 another 72 h (96 h AED) or 96 (120 h AED), 3rd instar larvae were prepared for dissection or pictures were taken
537 of whole larvae with a Leica MZ FLIII Fluorescence Stereomicroscope. For hid experiments, transferred larvae
538 were incubated for 197 h at 18°C, shifted to 29°C for 12 h and finally dissected. To exclude microbial
539 contamination and maintain germ-free conditions, BxGal4;;DrsGFP/UAS-Ras^{V12}-eggs were dechorionated with a
540 50% Sodium Hypochlorite solution (Fisher Scientific, 10401841) immediately after collection and transferred to
541 vials with apple-agar supplemented with Nipagin, Propionic acid and the same antibiotics as above. Larvae were
542 then analysed at 24 h and 48 h AED.

543

544 ***Drs reporter assay***

545 Replicates of *Drosophila* larvae (n=24 larvae·replicate^{-1}; N>6 replicates) at 96 h AED were screened for
546 Drs-GFP reporter signals. Three phenotypes were distinguished: (1.) "Full" SG pattern includes GFP signal across
547 the entire PP and GFP$^+$-cells with reduced intensity in the DP. (2.) "Partial" SG is GFP$^+$ throughout the PP, but
548 less pronounced in DP with reduced signal intensity and fewer GFP$^+$-cells. (3.) "None" phenotype lacks signal
549 throughout the entire gland. Distribution of phenotypes were scored per replicate and significance calculated for
550 the "None"-phenotype via Dunn's test after performing the Kruskal-Wallis rank sum test.

551

qPCR

553   Total RNA of dissected salivary glands was isolated with the RNAqueous-Micro Kit (ThermoFisher
554 Scientific, AM1931) and from whole larvae with the RNAqueous Kit (ThermoFisher Scientific, AM1912)
555 according to the instructors manual. Residual genomic DNA was digested with RNase-free DNaseI (ThermoFisher
556 Scientific, EN0521) and cDNA reverse transcribed with SuperscriptIII (ThermoFisher Scientific, 18080-093)
557 while using oligo(dT)$_{16}$-primer (ThermoFisher Scientific, 8080128). Quality of all prepared totalRNA-extractions
558 was evaluated on a 5 mM Guanidinium Thiocyanate-agarose gel, for optimization purposes on a BioRad Experion
559 system (RNA StdSens Assay, 7007153, 7007154) and totalRNA for sequencing was run on a 2100 Bioanalyzer
560 Instrument (Agilent Technologies, 5067-1511). qPCR reactions were set as technical triplicates with KAPA SYBR
561 FAST qPCR Master Mix (KR0389, v9.13) including 200 nM final concentration of forward and reverse primers
562 and run on a Rotor-Gene Q 2plex HRM machine (9001550). See supplementary file 2 for list of all used qPCR
563 primers.

564

RNASeq library preparation and analysis

566   To avoid variability and thus confounding influences among the various RNASeq sample groups, we
567 controlled rigorously for age of female parents, larval density to avoid larval crowding, age differences as well as
568 developmental age itself and bacterial influences by using axenic culture conditions.
569   Poly(A)-containing mRNA molecules from totalRNA-samples were purified with oligo(dT)-magnetic
570 beads, subsequently fragmented and cDNA synthesised with random primers using the TruSeq RNA Sample
571 Preparation Kit v2. Adapter ligation and PCR-amplification precede cluster formation with a cBot cluster
572 generation system. All samples were sequenced on a HiSeq 2500 Illumina Genome Sequencer as PE50. Reads
573 were pseudoaligned with kallisto (v0.44.0) to a transcriptome index derived from all *Drosophila* transcript
574 sequences of the dmel release r6.19. Subsequent analysis of transcript abundances was performed in R with sleuth
575 (v0.30.0) including principal component analysis for dimensionality reduction, statistical and differential
576 expression analysis based on the beta statistic derived from the wald test. Enriched gene ontology terms were
577 identified by calculating hypergeometric p-values via the GOstats (v2.48.0) R package. Gene IDs were converted
578 via the AnnotationDbi (v1.44.0) package and the reference provided with the org.Dm.eg.db (v3.7.0) database and
579 geneset intersections visualized as UpSetR plot (v1.3.3). Please, see the accompanied R markdown deposited on
580 GitHub for details (https://github.com/robertkrautz/sg_analysis).

581

Immunohistochemistry

583   Proximal parts of staged larvae were inverted in PBS, unnecessary organs removed and samples fixed in
584 4% paraformaldehyde for 20 min. Subsequently, samples were washed three times for each 10 min in PBS or
585 PBST (1% TritonX-100). Blocking was performed with 0.1% BSA in PBS (H2) or 5% BSA in PBST (anti-CC3,
586 anti-pJNK and anti-Dorsal). Samples were then incubated in primary antibodies dissolved in blocking buffer for
587 12 h at 4°C or 1 h at room temperature (RT). Primary antibodies comprised rabbit anti-cleaved caspase 3 (1:200,
588 Cell Signalling Technology, 9661), mouse anti-pJNK (1:250, Cell Signalling Technology, 9255), mouse anti-
589 Dorsal (1:50, DSHB, 7A4) and mouse anti-Hemese (1:5; gift from István Andó). After washing as prior to blocking,
590 secondary antibodies were applied together with DAPI (1:500; Sigma-Aldrich; D9542) and when necessary

Phalloidin-546 (1:500, Molecular probes, A22283) in blocking buffer for 1 h at RT. As secondary antibodies goat anti-Mouse-IgG-Alexa546 (H+L; 1:500; ThermoFisher Scientific; A-11030) and goat anti-Rabbit-IgG-Alexa568 (H+L; 1:500; ThermoFisher Scientific; A-11011) were employed. Final washing as prior to blocking preceded dissection of the samples in PBS and separation of salivary glands. Tissues were mounted in Fluoromount-G (SouthernBiotech) and analysed with a Zeiss LSM780 confocal microscope. Images were extracted with Zen software (Blue edition) for further processing either in Adobe Photoshop CS5 Extended (v12.0.4 x64) or Inkscape (v0.92).

Hemocyte- / pJNK- / CC3- quantification and size measurement

Pictures of stained glands were taken with a Zeiss Axioplan 2 microscope equipped with an ACHROPLAN 4x lens and a Hamamatsu ORCA-ER camera (C4742-95). Images were extracted with AxioVision software (v40V 4.8.2.0) and analysed with ImageJ. Cumulated area of hemocyte attachment, pJNK or CC3 fluorescence per SG or per SG part was filtered in the Red-channel and gland size determined by outlining glands, PPs or DPs with the 'Polygon selection'-tool. The distribution of hemocytes in *Drosophila* can be approximated by a natural logarithm, which required transformation of hemocyte attachment- and SG-areas before calculating ratios (Sorrentino, 2010). Normality across all samples of a particular genotype and where necessary separated by gland part (i.e., proximal or distal) or time (i.e., 96 h and 120 h AED) was evaluated with the Shapiro-Wilk-test and by bootstrapping via the fitdistrplus R package (v1.0.11). Significant differences between experimental groups were determined for pairwise comparisons via the Student's t-test after validating un-/equal variance via the Bartlett's test. Data and statistical analysis was performed in R.

Nuclei volume

Z-stacks of entire salivary glands were captured with a Zeiss LSM780 confocal microscope for DAPI signal. Obtained stacks were further processed in ImageJ via the '3D Object Counter' plugin. Proximal and distal compartments were defined with the 'Polygon selection'-tool. Transfer of the region of interest to all z-stack slices, signal thresholding, object identification and volume determination were integrated in a macro workflow. Data were plotted as average nucleus volume for all nuclei of individual glands or gland parts. Representative sections of individual z-stack slices showing the transition between proximal and distal compartments were cropped and added for illustration. Statistics were performed similar to the analysis of Hemocyte-, pJNK- and CC3-quantifications.

In situ hybridization

Proximal parts of staged larvae were separated from the larval body in PBS, transferred to fixative (4% PFA), washed 4 times for 15 min in PBS and stored at -20°C in methanol. A cDNA for the Drs locus (LP03851) was obtained from DGRC. Probe synthesis and detailed ISH procedure is described elsewhere (Hauptmann, 2015). Stained salivary glands were mounted in Fluoromount-G (SouthernBiotech) and images were captured with a Leica MZ16 microscope combined with a Leica DFC300Fx camera.

Acknowledgements

640

641   ***References***

642

643   Adamo, S.A. (2017). Stress responses sculpt the insect immune system, optimizing defense in
644   an ever-changing world. Dev Comp Immunol *66*, 24-32.
645   Ahmed-de-Prado, S., and Baonza, A. (2018). Drosophila as a Model System to Study Cell
646   Signaling in Organ Regeneration. Biomed Res Int *2018*, 7359267.
647   Ammeux, N., Housden, B.E., Georgiadis, A., Hu, Y., and Perrimon, N. (2016). Mapping
648   signaling pathway cross-talk in Drosophila cells. Proc Natl Acad Sci U S A *113*, 9940-9945.
649   Andersen, D.S., Colombani, J., Palmerini, V., Chakrabandhu, K., Boone, E., Rothlisberger,
650   M., Toggweiler, J., Basler, K., Mapelli, M., Hueber, A.O.*, et al.* (2015). The Drosophila TNF
651   receptor Grindelwald couples loss of cell polarity and neoplastic growth. Nature *522*, 482-
652   486.
653   Andrew, D.J., Henderson, K.D., and Seshaiah, P. (2000). Salivary gland development in
654   Drosophila melanogaster. Mech Dev *92*, 5-17.
655   Antebi, Y.E., Nandagopal, N., and Elowitz, M.B. (2017). An operational view of intercellular
656   signaling pathways. Curr Opin Syst Biol *1*, 16-24.
657   Araki, M., Awane, R., Sato, T., Ohkawa, Y., and Inoue, Y. (2018). Anti-tumor effects of
658   antimicrobial peptides, targets of the innate immune system, against hematopoietic tumors in
659   Drosophila mxc mutants. BioRxiv.
660   Babcock, D.T., Brock, A.R., Fish, G.S., Wang, Y., Perrin, L., Krasnow, M.A., and Galko,
661   M.J. (2008). Circulating blood cells function as a surveillance system for damaged tissue in
662   Drosophila larvae. P Natl Acad Sci USA *105*, 10017-10022.
663   Balkwill, F., and Mantovani, A. (2001). Inflammation and cancer: back to Virchow? Lancet
664   *357*, 539-545.
665   Bartkova, J., Horejsi, Z., Koed, K., Kramer, A., Tort, F., Zieger, K., Guldberg, P., Sehested,
666   M., Nesland, J.M., Lukas, C.*, et al.* (2005). DNA damage response as a candidate anti-cancer
667   barrier in early human tumorigenesis. Nature *434*, 864-870.
668   Bartkova, J., Rezaei, N., Liontos, M., Karakaidos, P., Kletsas, D., Issaeva, N., Vassiliou, L.V.,
669   Kolettas, E., Niforou, K., Zoumpourlis, V.C.*, et al.* (2006). Oncogene-induced senescence is
670   part of the tumorigenesis barrier imposed by DNA damage checkpoints. Nature *444*, 633-637.
671   Bergmann, A., Agapite, J., McCall, K., and Steller, H. (1998). The Drosophila gene hid is a
672   direct molecular target of Ras-dependent survival signaling. Cell *95*, 331-341.
673   Bilder, D., Li, M., and Perrimon, N. (2000). Cooperative regulation of cell polarity and
674   growth by Drosophila tumor suppressors. Science *289*, 113-116.

675   Britton, J.S., and Edgar, B.A. (1998). Environmental control of the cell cycle in Drosophila:
676   nutrition activates mitotic and endoreplicative cells by distinct mechanisms. Development
677   *125*, 2149-2158.
678   Buchon, N., Broderick, N.A., Poidevin, M., Pradervand, S., and Lemaitre, B. (2009).
679   Drosophila intestinal response to bacterial infection: activation of host defense and stem cell
680   proliferation. Cell Host Microbe *5*, 200-211.
681   Buchon, N., Silverman, N., and Cherry, S. (2014). Immunity in Drosophila melanogaster--
682   from microbial recognition to whole-organism physiology. Nat Rev Immunol *14*, 796-810.
683   Burnet, F.M. (1970). An immunological approach to ageing. Lancet *2*, 358-360.
684   Burnet, M. (1957). Cancer - a Biological Approach .1. The Processes of Control. Brit Med J
685   *1*, 779-786.
686   Chatterjee, N., and Bohmann, D. (2012). A versatile PhiC31 based reporter system for
687   measuring AP-1 and Nrf2 signaling in Drosophila and in tissue culture. PLoS One *7*, e34063.
688   Chovatiya, R., and Medzhitov, R. (2014). Stress, inflammation, and defense of homeostasis.
689   Mol Cell *54*, 281-288.
690   Colombani, J., Bianchini, L., Layalle, S., Pondeville, E., Dauphin-Villemant, C.,
691   Antoniewski, C., Carre, C., Noselli, S., and Leopold, P. (2005). Antagonistic actions of
692   ecdysone and insulins determine final size in Drosophila. Science *310*, 667-670.
693   Cordero, J.B., Macagno, J.P., Stefanatos, R.K., Strathdee, K.E., Cagan, R.L., and Vidal, M.
694   (2010). Oncogenic Ras diverts a host TNF tumor suppressor activity into tumor promoter.
695   Dev Cell *18*, 999-1011.
696   Di Micco, R., Fumagalli, M., Cicalese, A., Piccinin, S., Gasparini, P., Luise, C., Schurra, C.,
697   Garre, M., Nuciforo, P.G., Bensimon, A.*, et al.* (2006). Oncogene-induced senescence is a
698   DNA damage response triggered by DNA hyper-replication. Nature *444*, 638-642.
699   Edgar, B.A. (2006). How flies get their size: genetics meets physiology. Nat Rev Genet *7*,
700   907-916.
701   Edgar, B.A., Zielke, N., and Gutierrez, C. (2014). Endocycles: a recurrent evolutionary
702   innovation for post-mitotic cell growth (vol 15, pg 197, 2014). Nat Rev Mol Cell Bio *15*.
703   Eming, S.A. (2014). Evolution of immune pathways in regeneration and repair: recent
704   concepts and translational perspectives. Semin Immunol *26*, 275-276.
705   Enomoto, M., Kizawa, D., Ohsawa, S., and Igaki, T. (2015). JNK signaling is converted from
706   anti- to pro-tumor pathway by Ras-mediated switch of Warts activity. Dev Biol *403*, 162-171.
707   Fan, Y., and Bergmann, A. (2010). The cleaved-Caspase-3 antibody is a marker of Caspase-9-
708   like DRONC activity in Drosophila. Cell Death Differ *17*, 534-539.
709   Ferrandon, D., Jung, A.C., Criqui, M., Lemaitre, B., Uttenweiler-Joseph, S., Michaut, L.,
710   Reichhart, J., and Hoffmann, J.A. (1998a). A drosomycin-GFP reporter transgene reveals a
711   local immune response in Drosophila that is not dependent on the Toll pathway. EMBO J *17*,
712   1217-1227.
713   Ferrandon, D., Jung, A.C., Criqui, M., Lemaitre, B., Uttenweiler-Joseph, S., Michaut, L.,
714   Reichhart, J., and Hoffmann, J.A. (1998b). A drosomycin-GFP reporter transgene reveals a
715   local immune response in Drosophila that is not dependent on the Toll pathway. Embo J *17*,
716   1217-1227.
717   Fogarty, C.E., Diwanji, N., Lindblad, J.L., Tare, M., Amcheslavsky, A., Makhijani, K.,
718   Bruckner, K., Fan, Y., and Bergmann, A. (2016). Extracellular Reactive Oxygen Species
719   Drive Apoptosis-Induced Proliferation via Drosophila Macrophages. Curr Biol *26*, 575-584.
720   Fuse, Y., and Kobayashi, M. (2017). Conservation of the Keap1-Nrf2 System: An
721   Evolutionary Journey through Stressful Space and Time. Molecules *22*.
722   Galko, M.J., and Krasnow, M.A. (2004). Cellular and genetic analysis of wound healing in
723   Drosophila larvae. PLoS Biol *2*, E239.

724   Germani, F., Hain, D., Sternlicht, D., Moreno, E., and Basler, K. (2018). The Toll pathway
725   inhibits tissue growth and regulates cell fitness in an infection-dependent manner. Elife *7*.
726   Han, S.H., Ryu, J.H., Oh, C.T., Nam, K.B., Nam, H.J., Jang, I.H., Brey, P.T., and Lee, W.J.
727   (2004). The moleskin gene product is essential for Caudal-mediated constitutive antifungal
728   Drosomycin gene expression in Drosophila epithelia. Insect Mol Biol *13*, 323-327.
729   Hauling, T., Krautz, R., Markus, R., Volkenhoff, A., Kucerova, L., and Theopold, U. (2014).
730   A Drosophila immune response against Ras-induced overgrowth. Biol Open *3*, 250-260.
731   Hauptmann, G. (2015). In situ hybridization methods (New York: Humana Press).
732   Hawkins, C.J., Yoo, S.J., Peterson, E.P., Wang, S.L., Vernooy, S.Y., and Hay, B.A. (2000).
733   The Drosophila caspase DRONC cleaves following glutamate or aspartate and is regulated by
734   DIAP1, HID, and GRIM. J Biol Chem *275*, 27084-27093.
735   Hay, B.A., Wolff, T., and Rubin, G.M. (1994). Expression of Baculovirus P35 Prevents Cell-
736   Death in Drosophila. Development *120*, 2121-2129.
737   Herranz, H., Eichenlaub, T., and Cohen, S.M. (2016). Cancer in Drosophila: Imaginal Discs
738   as a Model for Epithelial Tumor Formation. Curr Top Dev Biol *116*, 181-199.
739   Herrera, S.C., Martin, R., and Morata, G. (2013). Tissue homeostasis in the wing disc of
740   Drosophila melanogaster: immediate response to massive damage during development. PLoS
741   Genet *9*, e1003446.
742   Herrera, S.C., and Morata, G. (2014). Transgressions of compartment boundaries and cell
743   reprogramming during regeneration in Drosophila. Elife *3*, e01831.
744   Hoffmann, A.A., and Parsons, P.A. (1991). Evolutionary genetics and environmental stress
745   (Oxford ; New York: Oxford University Press).
746   Igaki, T., Pagliarini, R.A., and Xu, T. (2006). Loss of cell polarity drives tumor growth and
747   invasion through JNK activation in Drosophila. Curr Biol *16*, 1139-1146.
748   Imler, J.L., and Bulet, P. (2005). Antimicrobial peptides in Drosophila: structures, activities
749   and gene regulation. Chem Immunol Allergy *86*, 1-21.
750   Jacob, L., Opper, M., Metzroth, B., Phannavong, B., and Mechler, B.M. (1987). Structure of
751   the l(2)gl gene of Drosophila and delimitation of its tumor suppressor domain. Cell *50*, 215-
752   225.
753   Jia, Q., Liu, Y., Liu, H., and Li, S. (2014). Mmp1 and Mmp2 cooperatively induce Drosophila
754   fat body cell dissociation with distinct roles. Sci Rep *4*, 7535.
755   Junell, A., Uvell, H., Davis, M.M., Edlundh-Rose, E., Antonsson, A., Pick, L., and Engstrom,
756   Y. (2010). The POU transcription factor Drifter/Ventral veinless regulates expression of
757   Drosophila immune defense genes. Mol Cell Biol *30*, 3672-3684.
758   Jung, H., Hsiung, B., Pestal, K., Procyk, E., and Raulet, D.H. (2012). RAE-1 ligands for the
759   NKG2D receptor are regulated by E2F transcription factors, which control cell cycle entry. J
760   Exp Med *209*, 2409-2422.
761   Kholodenko, B.N. (2006). Cell-signalling dynamics in time and space. Nat Rev Mol Cell Biol
762   *7*, 165-176.
763   Kim, M.J., and Choe, K.M. (2014). Basement membrane and cell integrity of self-tissues in
764   maintaining Drosophila immunological tolerance. PLoS Genet *10*, e1004683.
765   Kurada, P., and White, K. (1998). Ras promotes cell survival in Drosophila by
766   downregulating hid expression. Cell *95*, 319-329.
767   Kurata, S. (2004). Recognition of infectious non-self and activation of immune responses by
768   peptidoglycan recognition protein (PGRP)-family members in Drosophila. Developmental
769   and Comparative Immunology *28*, 89-95.
770   Lemaitre, B., and Hoffmann, J. (2007). The host defense of Drosophila melanogaster. Annu
771   Rev Immunol *25*, 697-743.

772   Liu, D., Shaukat, Z., Saint, R.B., and Gregory, S.L. (2015). Chromosomal instability triggers
773   cell death via local signalling through the innate immune receptor Toll. Oncotarget *6*, 38552-
774   38565.
775   Loboda, A., Damulewicz, M., Pyza, E., Jozkowicz, A., and Dulak, J. (2016). Role of
776   Nrf2/HO-1 system in development, oxidative stress response and diseases: an evolutionarily
777   conserved mechanism. Cell Mol Life Sci *73*, 3221-3247.
778   Lowe, S.W., Cepero, E., and Evan, G. (2004). Intrinsic tumour suppression. Nature *432*, 307-
779   315.
780   Mantovani, A., Allavena, P., Sica, A., and Balkwill, F. (2008). Cancer-related inflammation.
781   Nature *454*, 436-444.
782   Mason, D.X., Jackson, T.J., and Lin, A.W. (2004). Molecular signature of oncogenic ras-
783   induced senescence. Oncogene *23*, 9238-9246.
784   Medzhitov, R., and Janeway, C.A. (2002). Decoding the patterns of self and nonself by the
785   innate immune system. Science *296*, 298-300.
786   Meier, P., Silke, J., Leevers, S.J., and Evan, G.I. (2000). The Drosophila caspase DRONC is
787   regulated by DIAP1. EMBO J *19*, 598-611.
788   Meyer, S.N., Amoyel, M., Bergantinos, C., de la Cova, C., Schertel, C., Basler, K., and
789   Johnston, L.A. (2014). An ancient defense system eliminates unfit cells from developing
790   tissues during cell competition. Science *346*, 1258236.
791   Mirth, C.K., Tang, H.Y., Makohon-Moore, S.C., Salhadar, S., Gokhale, R.H., Warner, R.D.,
792   Koyama, T., Riddiford, L.M., and Shingleton, A.W. (2014). Juvenile hormone regulates body
793   size and perturbs insulin signaling in Drosophila. Proc Natl Acad Sci U S A *111*, 7018-7023.
794   Morin, X., Daneman, R., Zavortink, M., and Chia, W. (2001). A protein trap strategy to detect
795   GFP-tagged proteins expressed from their endogenous loci in Drosophila. Proc Natl Acad Sci
796   U S A *98*, 15050-15055.
797   Muzzopappa, M., Murcia, L., and Milan, M. (2017). Feedback amplification loop drives
798   malignant growth in epithelial tissues. Proc Natl Acad Sci U S A *114*, E7291-E7300.
799   Ohlstein, B., and Spradling, A. (2006). The adult Drosophila posterior midgut is maintained
800   by pluripotent stem cells. Nature *439*, 470-474.
801   Orr-Weaver, T.L. (2015). When bigger is better: the role of polyploidy in organogenesis.
802   Trends Genet *31*, 307-315.
803   Pagliarini, R.A., and Xu, T. (2003). A genetic screen in Drosophila for metastatic behavior.
804   Science *302*, 1227-1231.
805   Parisi, F., Stefanatos, R.K., Strathdee, K., Yu, Y., and Vidal, M. (2014). Transformed
806   epithelia trigger non-tissue-autonomous tumor suppressor response by adipocytes via
807   activation of Toll and Eiger/TNF signaling. Cell Rep *6*, 855-867.
808   Park, J.M., Brady, H., Ruocco, M.G., Sun, H., Williams, D., Lee, S.J., Kato, T., Jr., Richards,
809   N., Chan, K., Mercurio, F.*, et al.* (2004). Targeting of TAK1 by the NF-kappa B protein
810   Relish regulates the JNK-mediated immune response in Drosophila. Genes Dev *18*, 584-594.
811   Parvy, J.P., Yu, Y., Dostalova, A., Kondo, S., Kurjan, A., Bulet, P., Lemaitre, B., Vidal, M.,
812   and Cordero, J.B. (2019). The antimicrobial peptide Defensin cooperates with Tumor
813   Necrosis Factor to drive tumour cell death in Drosophila. BioRxiv.
814   Pastor-Pareja, J.C., Wu, M., and Xu, T. (2008). An innate immune response of blood cells to
815   tumors and tissue damage in Drosophila. Dis Model Mech *1*, 144-154; discussion 153.
816   Perez, E., Lindblad, J.L., and Bergmann, A. (2017). Tumor-promoting function of apoptotic
817   caspases by an amplification loop involving ROS, macrophages and JNK in Drosophila. Elife
818   *6*.
819   Pinal, N., Martin, M., Medina, I., and Morata, G. (2018). Short-term activation of the Jun N-
820   terminal kinase pathway in apoptosis-deficient cells of Drosophila induces tumorigenesis. Nat
821   Commun *9*, 1541.

822   Piper, M.D., Blanc, E., Leitao-Goncalves, R., Yang, M., He, X., Linford, N.J., Hoddinott,
823   M.P., Hopfen, C., Soultoukis, G.A., Niemeyer, C., *et al.* (2014). A holidic medium for
824   Drosophila melanogaster. Nat Methods *11*, 100-105.
825   Rämet, M., Lanot, R., Zachary, D., and Manfruelli, P. (2002). JNK signaling pathway is
826   required for efficient wound healing in *Drosophila*. Dev Biol *241*, 145-156.
827   Ramos-Lewis, W., and Page-McCaw, A. (2019). Basement membrane mechanics shape
828   development: Lessons from the fly. Matrix Biology *75-76*, 72-81.
829   Rankin, L.C., and Artis, D. (2018). Beyond Host Defense: Emerging Functions of the
830   Immune System in Regulating Complex Tissue Physiology. Cell *173*, 554-567.
831   Ryu, J.H., Kim, S.H., Lee, H.Y., Bai, J.Y., Nam, Y.D., Bae, J.W., Lee, D.G., Shin, S.C., Ha,
832   E.M., and Lee, W.J. (2008). Innate immune homeostasis by the homeobox gene caudal and
833   commensal-gut mutualism in Drosophila. Science *319*, 777-782.
834   Ryu, J.H., Nam, K.B., Oh, C.T., Nam, H.J., Kim, S.H., Yoon, J.H., Seong, J.K., Yoo, M.A.,
835   Jang, I.H., Brey, P.T., *et al.* (2004). The homeobox gene Caudal regulates constitutive local
836   expression of antimicrobial peptide genes in Drosophila epithelia. Mol Cell Biol *24*, 172-185.
837   Santabarbara-Ruiz, P., Lopez-Santillan, M., Martinez-Rodriguez, I., Binagui-Casas, A., Perez,
838   L., Milan, M., Corominas, M., and Serras, F. (2015). ROS-Induced JNK and p38 Signaling Is
839   Required for Unpaired Cytokine Activation during Drosophila Regeneration. PLoS Genet *11*,
840   e1005595.
841   Schmiedel, D., and Mandelboim, O. (2018). NKG2D Ligands-Critical Targets for Cancer
842   Immune Escape and Therapy. Front Immunol *9*, 2040.
843   Schuster, K.J., and Smith-Bolton, R.K. (2015). Taranis Protects Regenerating Tissue from
844   Fate Changes Induced by the Wound Response in Drosophila. Dev Cell *34*, 119-128.
845   Shim, J. (2015). Drosophila blood as a model system for stress sensing mechanisms. Bmb
846   Rep *48*, 223-228.
847   Shim, J., Gururaja-Rao, S., and Banerjee, U. (2013). Nutritional regulation of stem and
848   progenitor cells in Drosophila. Development *140*, 4647-4656.
849   Shlevkov, E., and Morata, G. (2012). A dp53/JNK-dependant feedback amplification loop is
850   essential for the apoptotic response to stress in Drosophila. Cell Death Differ *19*, 451-460.
851   Smith, A.V., and Orr-Weaver, T.L. (1991). The regulation of the cell cycle during Drosophila
852   embryogenesis: the transition to polyteny. Development *112*, 997-1008.
853   Sorrentino, R.P. (2010). Large standard deviations and logarithmic-normality: the truth about
854   hemocyte counts in Drosophila. Fly (Austin) *4*, 327-332.
855   Stevens, L.J., and Page-McCaw, A. (2012). A secreted MMP is required for
856   reepithelialization during wound healing. Mol Biol Cell *23*, 1068-1079.
857   Strand, D., Jakobs, R., Merdes, G., Neumann, B., Kalmes, A., Heid, H.W., Husmann, I., and
858   Mechler, B.M. (1994). The Drosophila Lethal(2)Giant Larvae Tumor-Suppressor Protein
859   Forms Homo-Oligomers and Is Associated with Nonmuscle Myosin-Ii Heavy-Chain. Journal
860   of Cell Biology *127*, 1361-1373.
861   Stronach, B.E., and Perrimon, N. (1999). Stress signaling in Drosophila. Oncogene *18*, 6172-
862   6182.
863   Takehana, A., Yano, T., Mita, S., Kotani, A., Oshima, Y., and Kurata, S. (2004).
864   Peptidoglycan recognition protein (PGRP)-LE and PGRP-LC act synergistically in
865   Drosophila immunity. Embo J *23*, 4690-4700.
866   Y. Tamori, W. M. Deng, Compensatory cellular hypertrophy: the other strategy for
867   tissuehomeostasis, Trends Cell Biol 24(2014) 230-237.
868   Tzou, P., Ohresser, S., Ferrandon, D., Capovilla, M., Reichhart, J.M., Lemaitre, B.,
869   Hoffmann, J.A., and Imler, J.L. (2000). Tissue-specific inducible expression of antimicrobial
870   peptide genes in Drosophila surface epithelia. Immunity *13*, 737-748.

871   Uhlirova, M., and Bohmann, D. (2006). JNK- and Fos-regulated Mmp1 expression cooperates
872   with Ras to induce invasive tumors in Drosophila. Embo J *25*, 5294-5304.
873   Uhlirova, M., Jasper, H., and Bohmann, D. (2005). Non-cell-autonomous induction of tissue
874   overgrowth by JNK/Ras cooperation in a Drosophila tumor model. Proc Natl Acad Sci U S A
875   *102*, 13123-13128.
876   Vantourout, P., Willcox, C., Turner, A., Swanson, C.M., Haque, Y., Sobolev, O., Grigoriadis,
877   A., Tutt, A., and Hayday, A. (2014). Immunological visibility: posttranscriptional regulation
878   of human NKG2D ligands by the EGF receptor pathway. Sci Transl Med *6*, 231ra249.
879   Vermeulen, C.J., and Loeschcke, V. (2007). Longevity and the stress response in Drosophila.
880   Exp Gerontol *42*, 153-159.
881   Vidal, M. (2010). The dark side of fly TNF: an ancient developmental proof reading
882   mechanism turned into tumor promoter. Cell Cycle *9*, 3851-3856.
883   Wagner, C., Isermann, K., and Roeder, T. (2009). Infection induces a survival program and
884   local remodeling in the airway epithelium of the fly. FASEB J *23*, 2045-2054.
885   Wu, C., Chen, C., Dai, J., Zhang, F., Chen, Y., Li, W., Pastor-Pareja, J.C., and Xue, L. (2015).
886   Toll pathway modulates TNF-induced JNK-dependent cell death in Drosophila. Open Biol *5*,
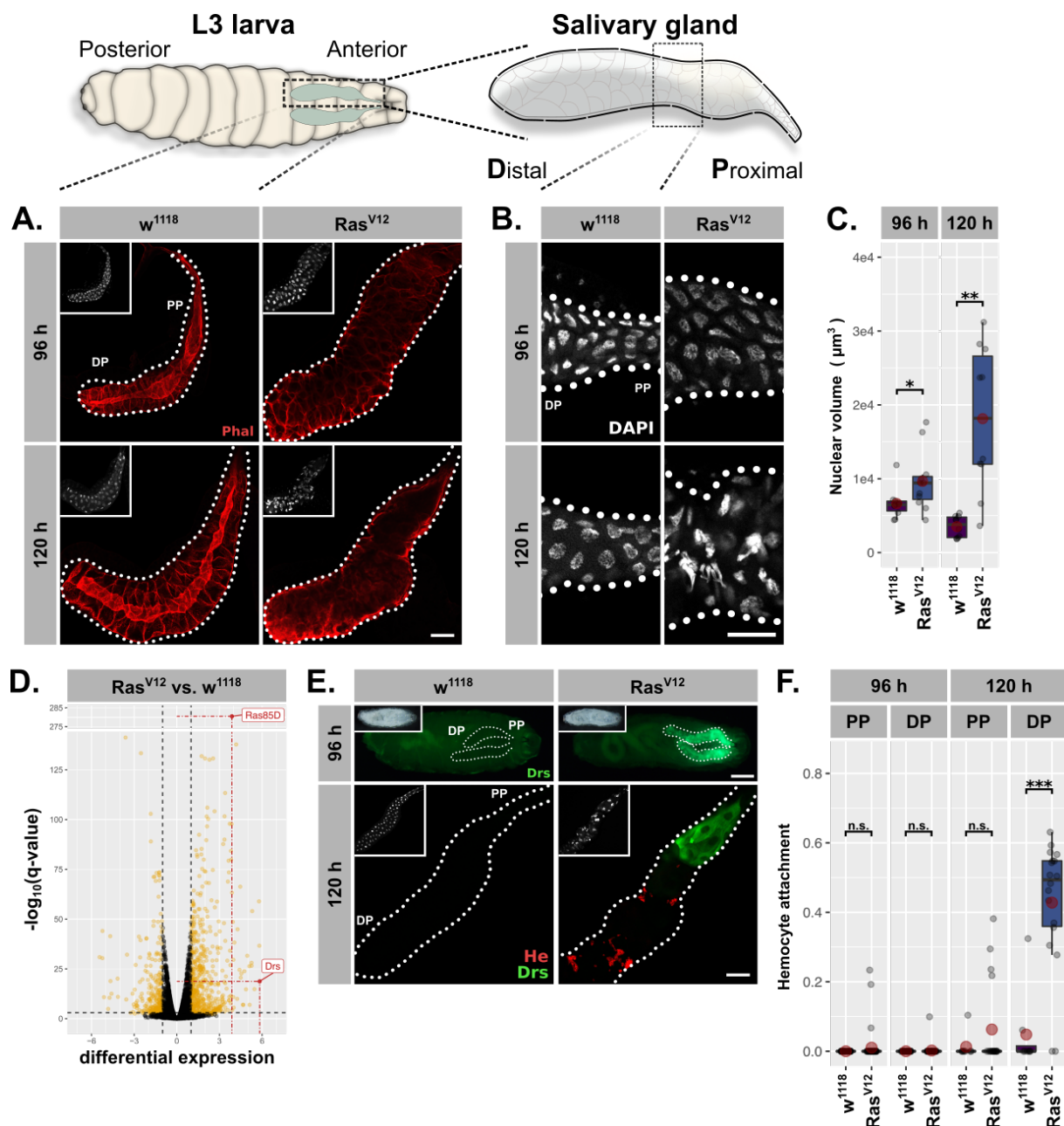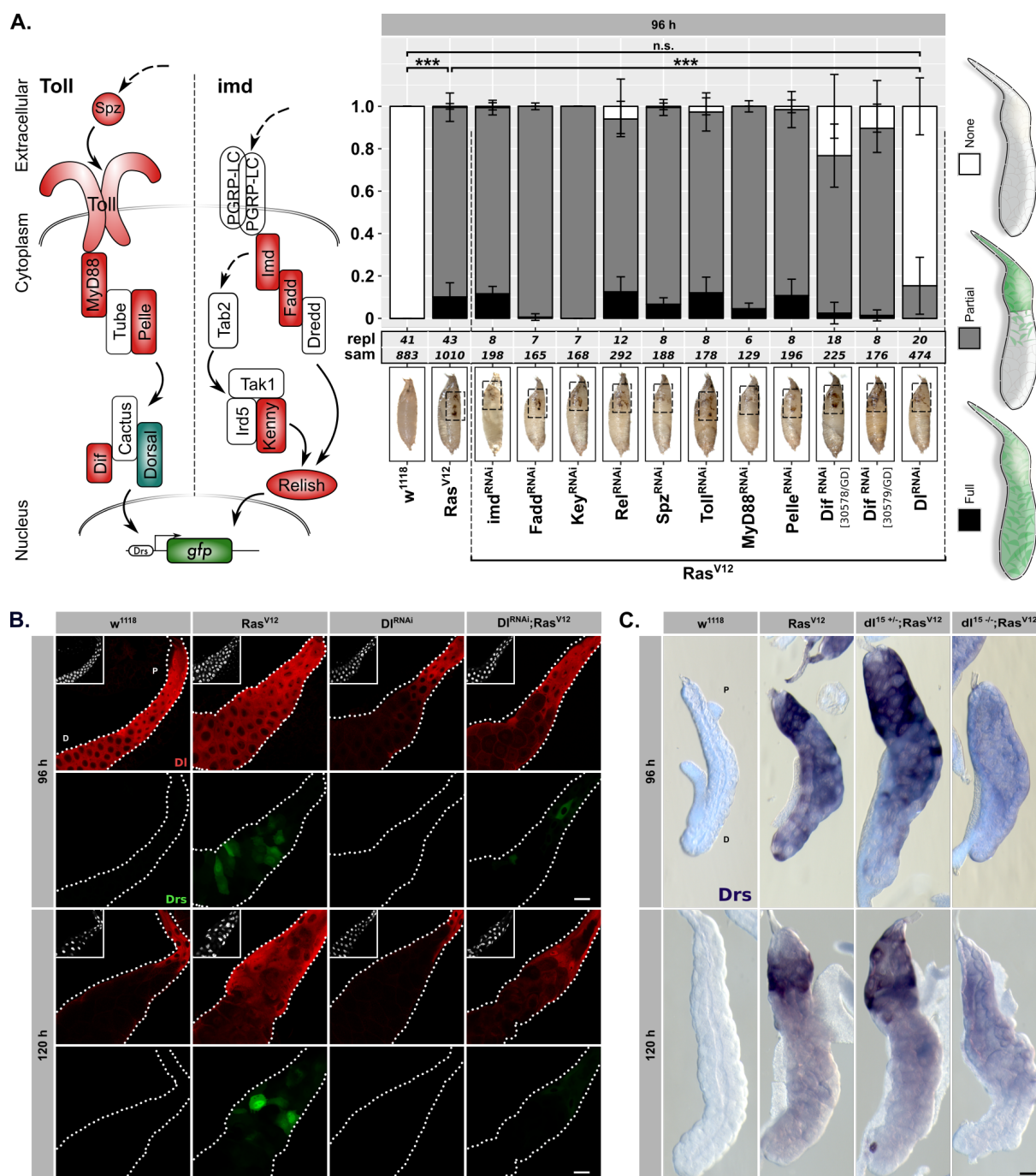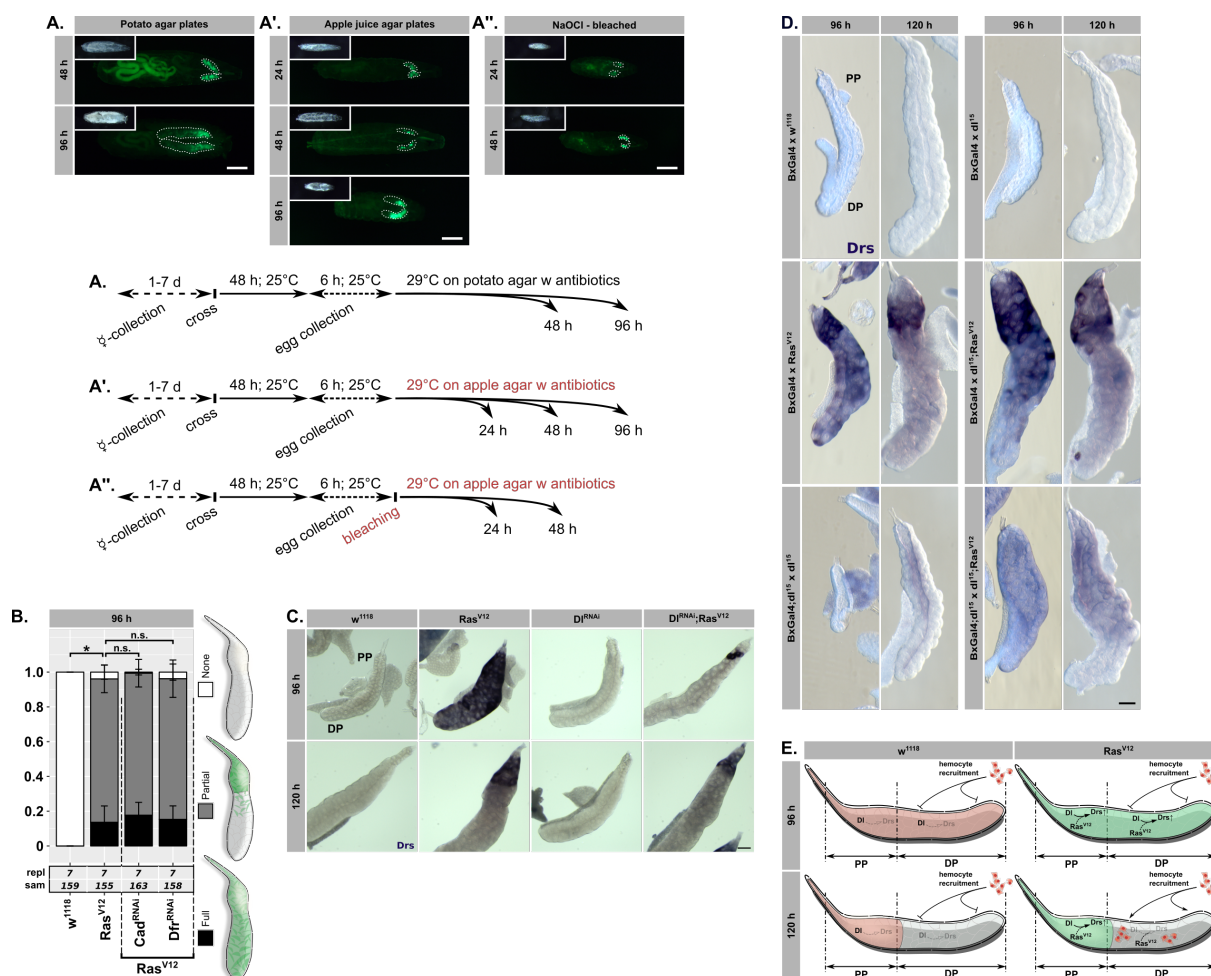887   140171.
888

Figure 1. *Ras^{V12}*-induced hypertrophy induces local and systemic immune responses (A.) *Ras^{V12}*-glands and controls stained with Phalloidin (red) to monitor tissue integrity at 96 h and 120 h AED. (B.) Nuclei stained with DAPI (white) to visualize nuclear volume and disintegration at 120 h AED in *Ras^{V12}*-glands. (C.) Nuclear volume as quantified by z-stacks of DAPI-stained SGs at 96 h and 120 h AED and averaged per gland. (D.) Comparative transcriptome analysis of *Ras^{V12}*-vs.-*w^{1118}*-glands. Differential expression quantified as beta statistic with q-values by wald test. Significantly differentially expressed genes (*log2(beta)≥1*; *q-value≤0.05*) highlighted in yellow. (E.) Upper: Whole larvae with DrsGFP reporter (green) expressing *Ras^{V12}* in glands or controls at 96 h AED. Lower: *Ras^{V12}*- and control-glands with DrsGFP reporter (green) stained for hemocytes (anti-Hemese, red). (F.) Hemocyte attachment measured as *ln(Hemese-area)/ln(SG-area)* and separated by time and gland part. Insets: (A./E. Lower) DAPI, (E. Upper) brightfield. Scalebars: (A./B./E. Lower) 100 μm, (E. Upper) 500 μm. Boxplots in (C./F.): lower/upper hinges indicate 1st/3rd quartiles, whisker lengths equal 1.5*IQR, red circle and bar represent mean and median. Significance evaluated by Student's t-tests (*** *p<0.001*, ** *p<0.01*, * *p<0.05*, n.s. *p≥0.05*).
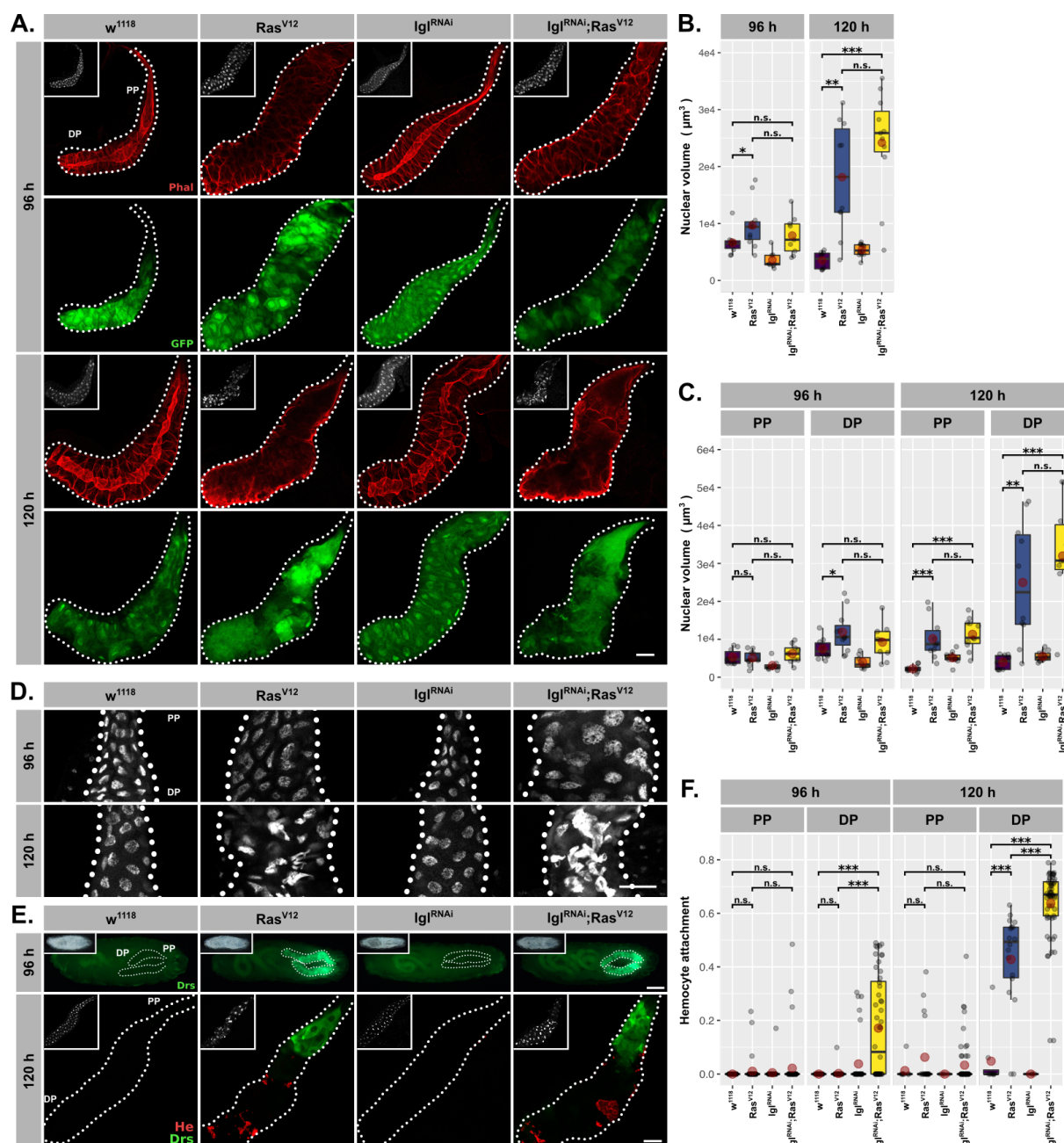
Supplemental Figure 1. (A.) GFP (green) expression to validate Bx^{MS1096} driver at 96 h and 120 h AED in all genotypes and Phalloidin (red) staining to trace tissue integrity. (B.) Volume of DAPI-stained nuclei derived from SG z-stacks and averaged per gland. (C.) Nuclear volume separated per gland into DP and PP. (D.) SG nuclei stained with DAPI (white) to indicate nuclear size and disintegration. (E.) Upper: Whole larvae carrying DrsGFP reporter (green). Lower: SGs with DrsGFP reporter signal (green) and stained hemocytes (anti-Hemese, red). (F.) Attached hemocytes quantified as *ln(Hemese-area)/ln(SG-area)* separated for DP and PP. Insets: (A./E. Lower) DAPI, (E. Upper) brightfield. Scalebars: (A./D./E. Lower) 100 μm, (E. Upper) 500 μm. Boxplots in (B./C./F.): lower/upper hinges indicate 1st/3rd quartiles, whisker lengths equal 1.5*IQR, red circle and bar represent mean and median. Significance evaluated by Student's t-tests (*** $p<0.001$, ** $p<0.01$, * $p<0.05$, n.s. $p≥0.05$). (A.-B./D.-E.) w^{1118} and Ras^{V12} data reused from Fig1. (C.) Separated nuclei measurements based on data in (B.). (F.) Separated hemocyte attachment measurements based on data in Fig1F.

915

916 **Figure 2. Drs expression is part of a genuine tissue-autonomous immune response** (A.) Semi quantitative

917 DrsGFP reporter assay to identify upstream effectors of Drs expression by RNAi in Ras^{V12}-glands. Schematic

918 representation (left) of the Toll-/Imd-pathways showing components with (green) and without an effect (red). The

919 3 distinguished phenotypes (right) were scored per replicate, means and standard deviations plotted (middle) and

920 p-values for "None"-phenotype calculated via Dunn's test based on Kruskal-Wallis rank sum test (*** $p<0.001$,

921 $n.s.$ $p\geq0.05$). Monitoring melanisation in pupae (insets) confirmed Ras^{V12}-expression to avoid false positives

922 (Hauling et al., 2014). (B.) Dorsal staining (red) and DrsGFP signal (green) in Ras^{V12}-glands with and without

923 Dorsal knock-down. (C.) In-$situ$ hybridization for endogenous Drs in Ras^{V12}-glands hetero- or homozygous mutant

924 for Dorsal (dl[15]). Insets: (B.) DAPI. Scalebars: (B./C.) 100 μm.

925

926

Supplemental Figure 2. Larvae with Ras^{V12}-glands and DrsGFP reporter (green) (A.) raised on plates with standard potatomash/molasses medium including stringent antibiotics cocktail, (A.') transferred immediately after hatching to germ- and yeast-extract free apple-agar supplemented with antibiotics or (A.'') after egg dechorionization were raised on sterile apple-agar including antibiotics. (B.) DrsGFP reporter assay with RNAi constructs against Caudal and Drifter in Ras^{V12}-glands. Sketched phenotypes (right) were scored, their mean and standard deviations plotted. Dunn's test performed to evaluate significant differences in distribution of "None"-phenotype (* $p<0.05$, n.s. $p\geq0.05$). (C.) Endogenous Drs mRNA detected by *in-situ* hybridization in Ras^{V12}-glands with or without knocking down Dorsal. (D.) Complete set of experimental genotypes for Drs *in-situ* hybridization as shown in Fig2C including additional controls. (E.) Schematic representation of endogenous, spatio-temporally regulated Dorsal expression pattern in SGs and its interaction with Ras^{V12} to promote Drs expression. Separation of Ras^{V12}-glands becomes apparent at 120 h AED with Drs-expression in PP and hemocyte recruitment to DP surface.
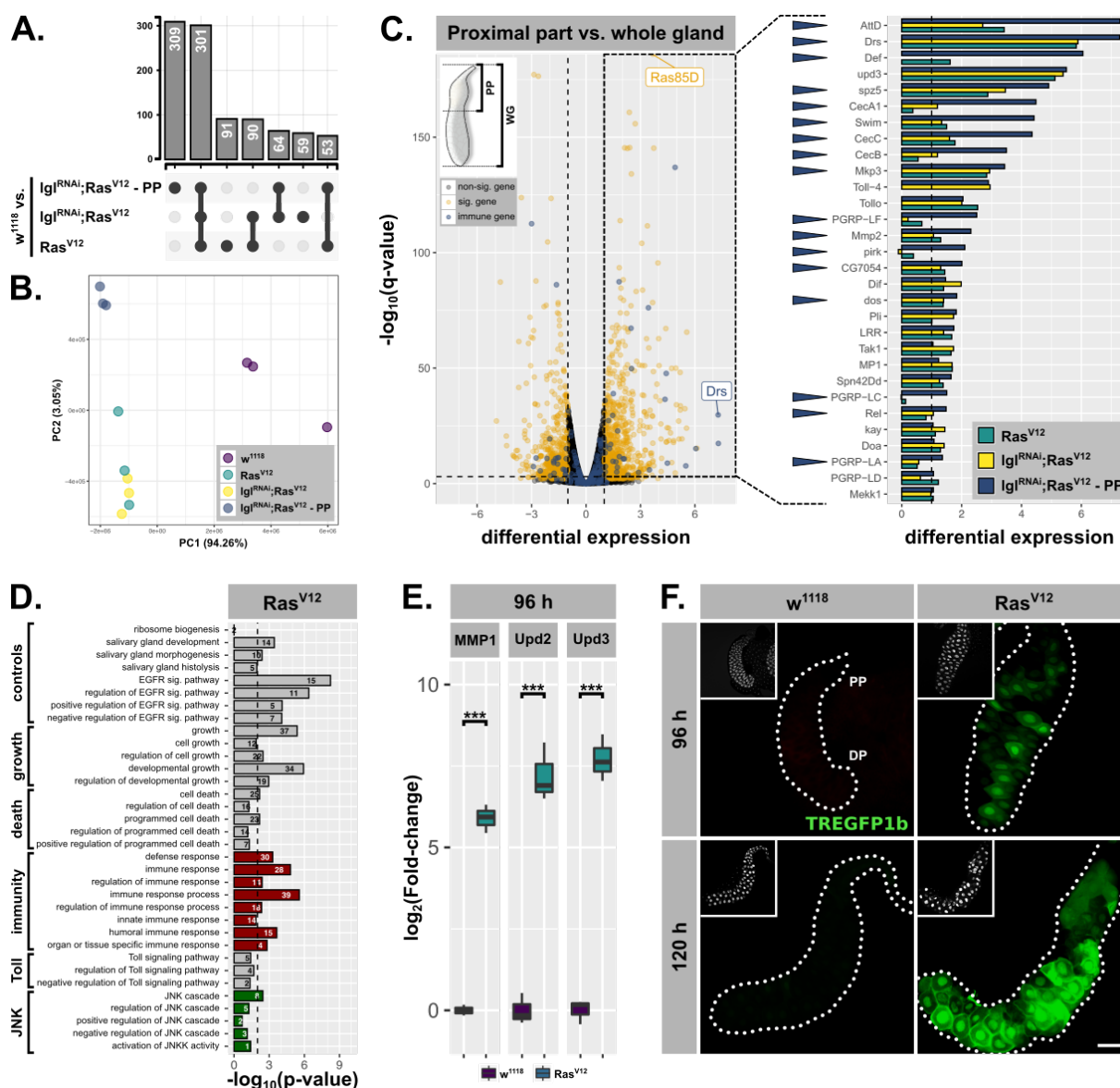
939

Figure 3. Hypertrophic *Ras^V12*-glands induce parallel immune and stress responses (A.) Common and specific genesets significantly upregulated (*log2(beta)≥1*; *q-value≤0.05*) in either *Ras^V12*, *lgl^RNAi;Ras^V12* or *lgl^RNAi;Ras^V12*-PP compared to *w^1118*-glands. (B.) PCA including all transcriptome replicates of all sequenced genotypes. (C.) Left: Comparative transcriptome analysis between PP of *lgl^RNAi;Ras^V12*- and entire *w^1118*-glands. Significantly differentially expressed genes (*log2(beta)≥1*; *q-value≤0.05*) and genes belonging to GO-term 'immune response' (GO:0006955) highlighted in yellow and blue. Right: Gene expression in *Ras^V12*, *lgl^RNAi;Ras^V12* or *lgl^RNAi;Ras^V12*-PP compared to *w^1118*-glands for immune genes significantly upregulated in the PP. Blue arrows indicate strongest expression in the PP for the indicated genes between all three groups. (D.) GO term enrichment among significantly upregulated genes in *Ras^V12*-glands including terms related to activation of JNK (green) and immune responses (red). Numbers in bars indicate amount of upregulated genes belonging to associated GO term. (E.) qPCR results for canonical JNK target genes (*log2*-transformed, fold-change over *Rpl32*) at 96 h AED. Lower/upper hinges of boxplots indicate 1st/3rd quartiles, whisker lengths equal 1.5*IQR and bar represents median. Significance evaluated by Student's t-tests (*** *p<0.001*). (F.) TREGFP1b reporter (green) signal in *Ras^V12*- and control-glands at 96 h and 120 h AED. Scalbar: 100 μm.
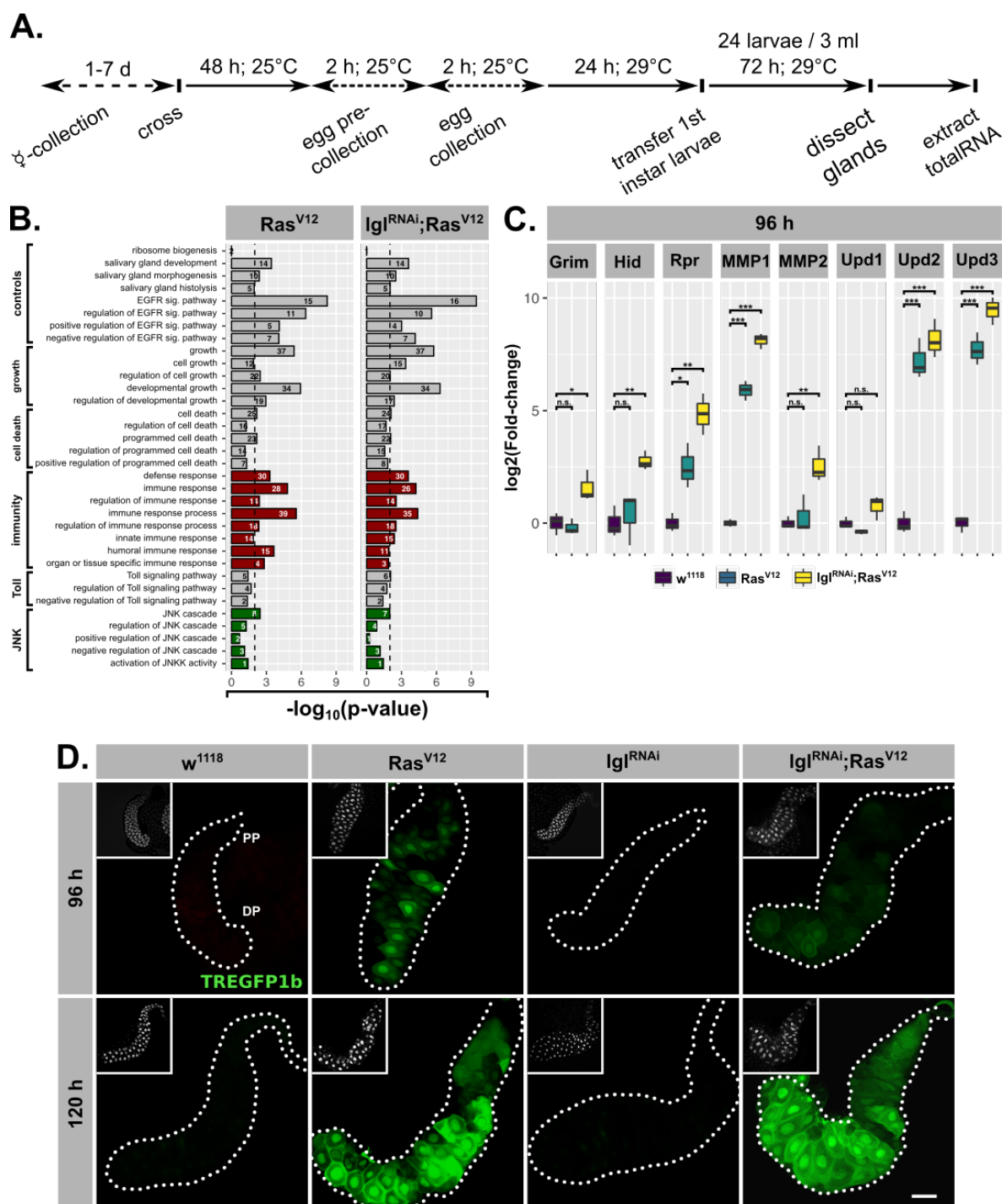
956
957 **Supplemental Figure 3.** (A.) Schematic overview of protocol for preparing tissues analysed by RNAseq. (B.)
958 Comparative GO term enrichment analysis for genes significantly upregulated in either *Ras^V12*- or *lgl^RNAi;Ras^V12*-
959 glands. Terms associated with activation of JNK (green) or immune response (red) are highlighted. GO terms for
960 *Ras^V12* also shown in Fig3D. (C.) Gene expression for canonical target genes measured by qPCR (*log2*-transformed,
961 fold-change over *Rpl32*). Lower/upper hinges of boxplots indicate 1st/3rd quartiles, whisker lengths equal 1.5*IQR
962 and bar represents median. Significance evaluated by Student's t-tests (*** *p<0.001*, ** *p<0.01*, * *p<0.05, n.s.
963 *p≥0.05)*. Results for MMP1, Upd2 and Upd3 in *Ras^V12*- and *w^1118*-glands also presented in Fig3E. (D.) Activation
964 of TREGFP1b reporter (green) used to evaluate induction of JNK-signalling at 96 h and 120 h AED. *Ras^V12*- and
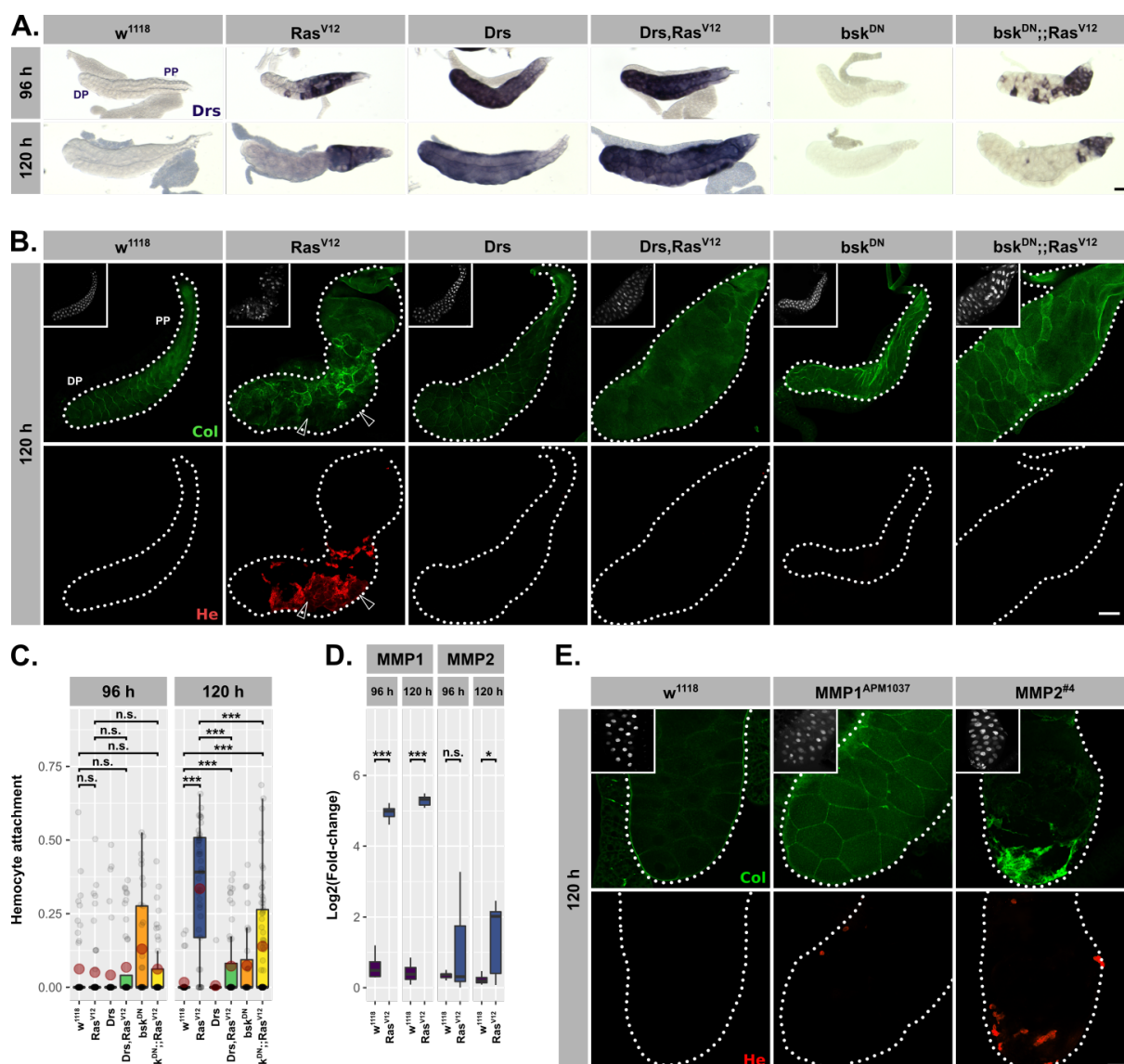965 *w^1118*-images also presented in Fig3F. Scalebar: 100 μm.

966

967 **Figure 4. Drs overexpression and JNK inhibition individually prevent tissue disintegration** (A.) Drs-specific
968 *in-situ* hybridization identifies endogenous (Ras^{V12} / bsk^{DN};;Ras^{V12}) and exogenous (Drs / Drs,Ras^{V12}) Drs
969 expression. (B.) Collagen-GFP trap (vkg^{G00454}, green) and Hemese staining (red) identify integrity of BM and
970 hemocyte attachment to gland surface. Arrows indicate BM-free areas occupied by hemocytes. (C.) Hemocyte
971 attachment at 96 h and 120 h AED represented as *ln(Hemese-area)/ln(SG-area)*. (D.) *log2*-transformed, *Rpl32*-
972 normalized gene expression values obtained by qPCR at 96 h and 120 h AED. (E.) Visualization of BM by
973 Collagen-GFP trap (green) and Hemese-stained hemocytes (red) attached to the gland surface upon sole MMP1-
974 or MMP2-overexpression. Insets: (B./E.) DAPI. Scalebars: (A./B./E.) 100 µm. Boxplots in (C./D.): lower/upper
975 hinges indicate 1st/3rd quartiles, whisker lengths equal 1.5*IQR, red circle and bar represent mean and median.
976 Significance evaluated by Student's t-tests (*** *p<0.001, ** p<0.01, * p<0.05, n.s. p≥0.05)*.

977
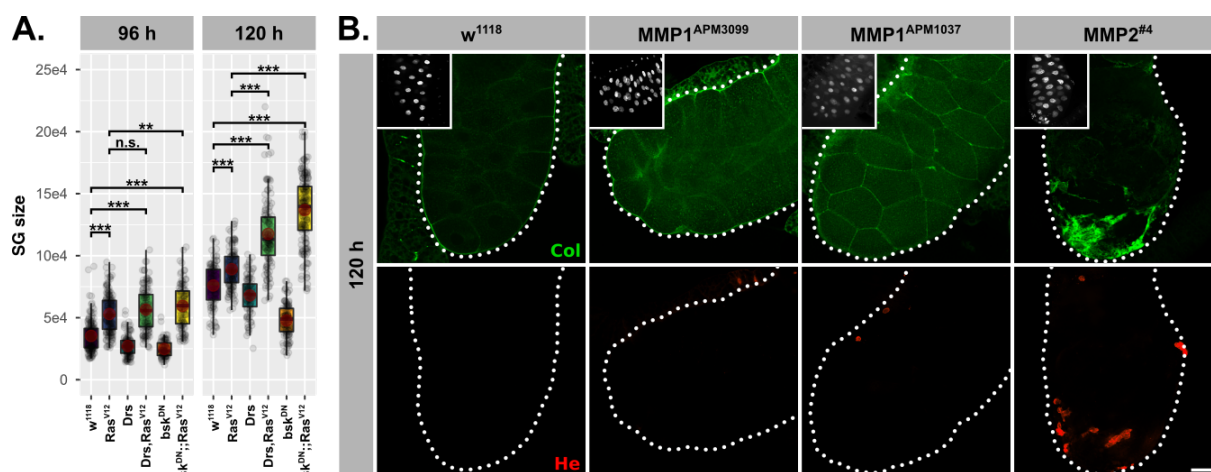
Supplemental Figure 4. (A.) SG size measured as outlined area in captured images at 96 h and 120 h AED. Lower/upper hinges of boxplots indicate $1^{st}/3^{rd}$ quartiles, whisker lengths equal 1.5*IQR, red circle and bar represent mean and median. Significance evaluated by Student's t-tests (*** *p<0.001*, ** *p<0.01*, * *p<0.05, n.s. p≥0.05*). (B.) Staining of BM via Collagen-GFP trap and attached hemocytes via Hemese antibody upon MMP1- or MMP2-overexpression. Images for MMP1[APM1037] and MMP2[#4] shown in Fig4E. Scalebar represents 100 μm and insets show DAPI staining.
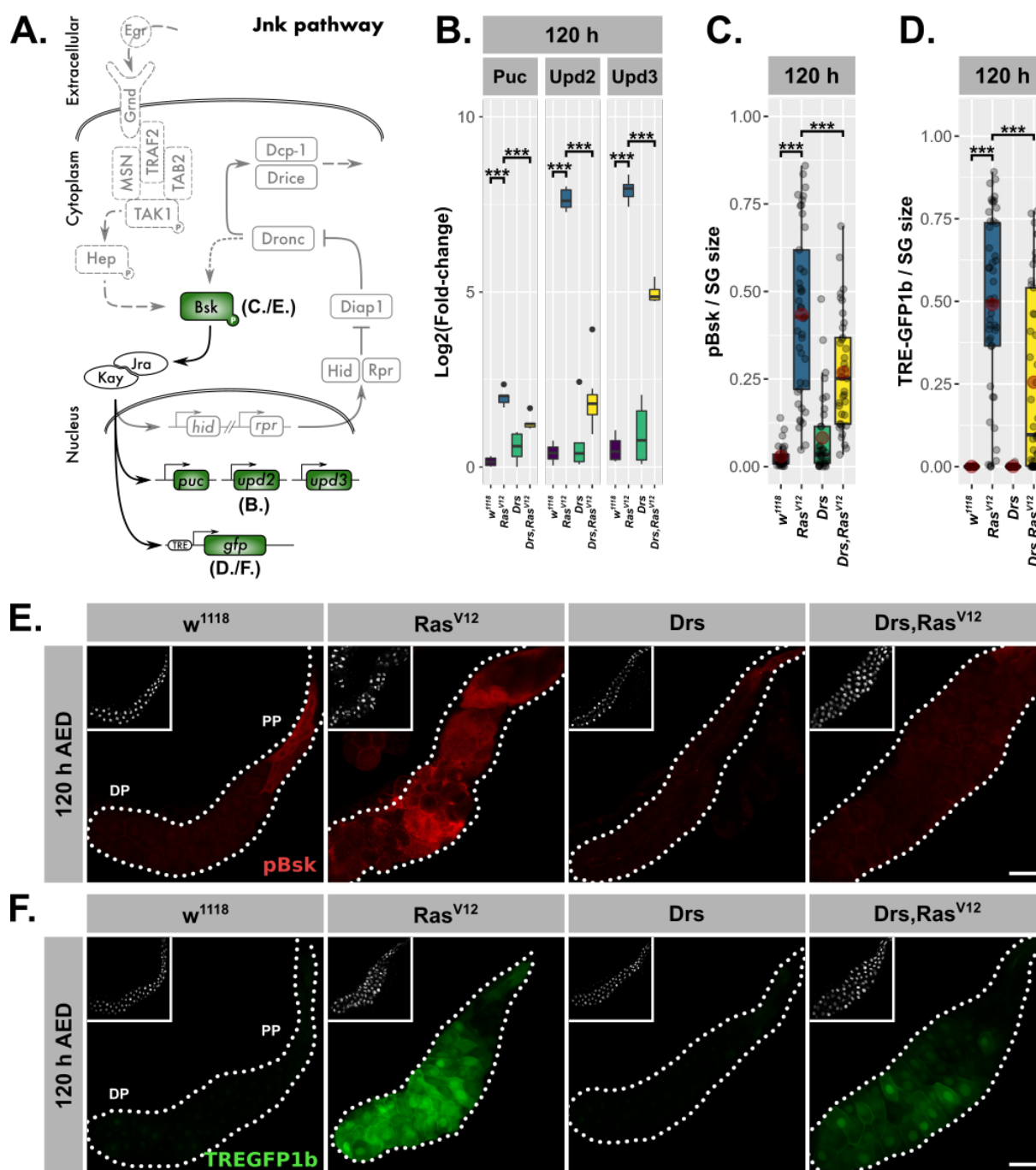
Figure 5. Drs overexpression inhibits JNK-activation (A.) Schematic representation of the JNK-pathway including read-outs (green) employed to track its activation. (B.) qPCR results for canonical JNK-target genes (*log2*-transformed, fold-change over *Rpl32*) at 120 h AED. (C.) Quantification of activated basket by staining with phosphorylation sensitive antibody per gland normalized for the SG size at 120 h AED. (D.) Quantification of TREGFP1b signal per gland normalized for SG size indicating JNK-dependent transcriptional activation at 120 h AED. (E.) Visualization of phosphorylated basket in *Ras^{V12}*-glands with and without Drs coexpression. (F.) Distribution of TREGFP1b reporter signal in *Ras^{V12}*-glands in the presence or absence of coexpressed Drs. Insets: (E./F.) DAPI. Scalebars: (E./F.) 100 μm. Boxplots in (B./C./D.): lower/upper hinges indicate 1st/3rd quartiles, whisker lengths equal 1.5*IQR, red circle and bar represent mean and median. Significance evaluated by Student's t-tests (*** *p<0.001, ** p<0.01, * p<0.05, n.s. p≥0.05)*.

998
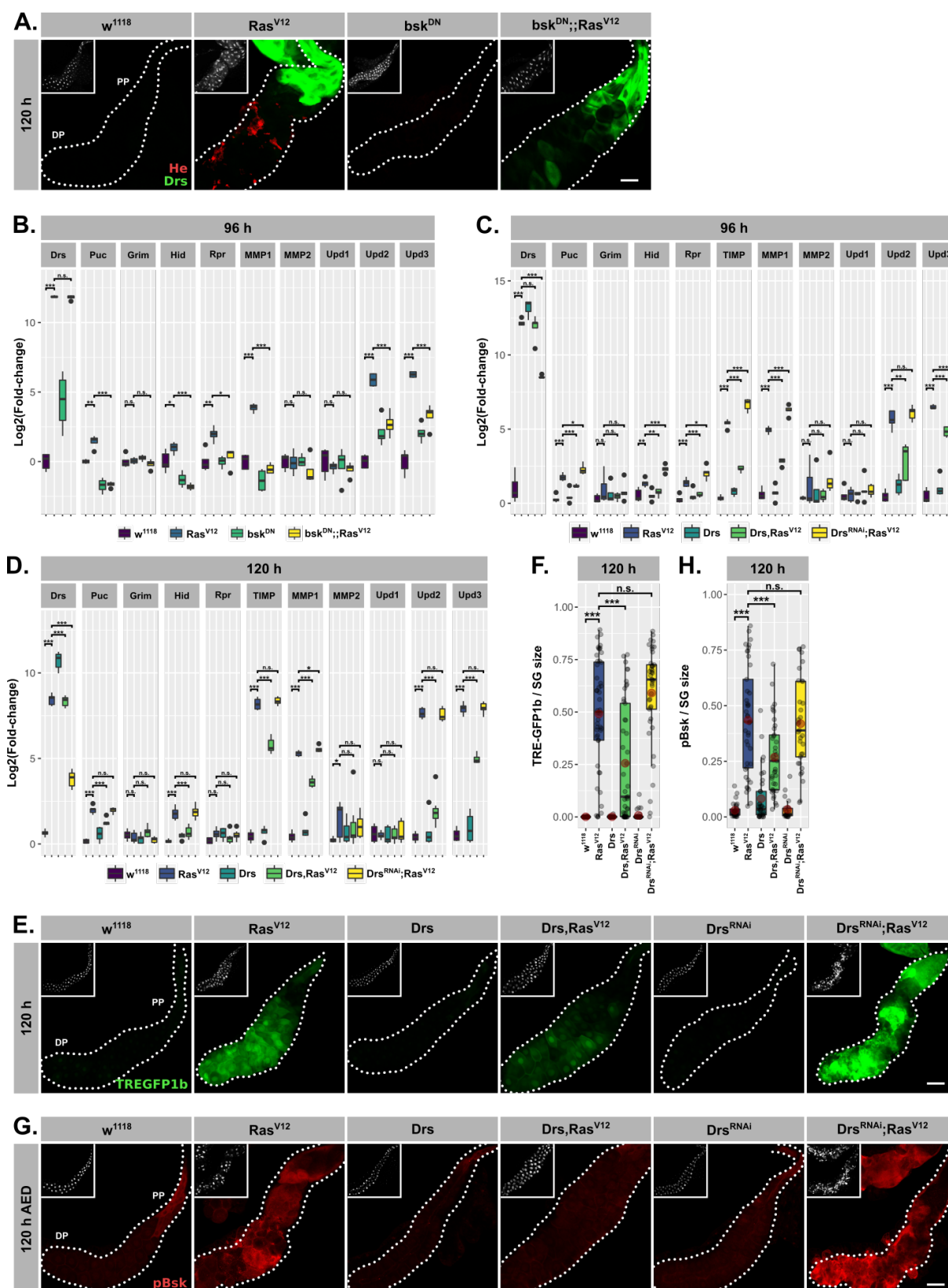
999 **Supplemental Figure 5.** (A.) DrsGFP reporter (green) and Hemese antibody (red) used to detect endogenous Drs

1000 expression and attached hemocytes. Expression of Drs and JNK-target genes as measured by qPCR (*log2*-

1001 transformed; normalized to *Rpl32* expression) in *Ras^V12*-glands (B.) with and without inhibited JNK-pathway at

1002 96 h AED, (C.) with and without Drs overexpression at 96 h AED and (D.) with and without Drs overexpression

1003 at 120 h AED. *Ras^V12*-glands with in- (Drs) or decreased (Drs^RNAi) Drs expression (E.) including TREGFP1b

1004 reporter (green) used to detect JNK-dependent transcriptional activation and (F.) corresponding quantifications of

1005 reporter signal normalized for SG size. Ras^{V12}-glands with in- (Drs) or decreased (Drs^{RNAi}) Drs expression (G.)

1006 stained for activated basket with a phosphorylation sensitive antibody (pBsk) and (H.) corresponding

1007 quantifications of detected signal normalized for SG size. Insets: (A./E./G.) DAPI. Scalebars: (A./E./G.) 100 µm.

1008 Boxplots in (B./C./D./F./H.): lower/upper hinges indicate 1st/3rd quartiles, whisker lengths equal 1.5*IQR, red

1009 circle and bar represent mean and median. Significance evaluated by Student's t-tests (*** *p<0.001*, ** *p<0.01*, *

1010 *p<0.05, n.s. p≥0.05)*. MMP1 and MMP2 expression in (C./D.) for w^{1118}- and Ras^{V12}-glands also shown in Fig4D.

1011 Hid expression in (C./D.) also presented in Fig6A. Images for w^{1118} / Ras^{V12} / Drs / Drs,Ras^{V12} in (E./G.) also

1012 presented in Fig5E./F.

1013

Figure 6. Drs inhibits programmed cell death (A.) Hid expression as measured by qPCR and plotted as *log2*-transformed values normalized to *Rpl32*-expression in *Ras^{V12}*-glands with in- (Drs) or decreased (Drs^{RNAi}) Drs expression. (B.) Schematic representation of the JNK-pathway including levels of employed interference (green). (C.) Nuclear volumina derived from z-stacks of DAPI-stained SGs and averaged per gland at 96 h and 120 h AED. (D.) DAPI stained (white) SG nuclei to indicate nuclear size and disintegration. *Ras^{V12}*-glands with in- (Drs) or decreased (Drs^{RNAi}) Drs expression (E.) stained with anti-CC3-antibody to detect Dronc activation (red) and (F.) corresponding quantifications of detected signal normalized for SG size. Insets in (E.) show DAPI and scalebars in (D./E.) represent 100 µm. Lower/upper hinges of boxplots in (A./C./F.) indicate 1st/3rd quartiles, whisker lengths equal 1.5*IQR, red circle and bar represent mean and median. Significance evaluated by Student's t-tests (*** *p<0.001)*.

1026

1027 **Supplemental Figure 6.** (A.) Ras^{V12}-glands with in- (Drs) or decreased (Drs^{RNAi}) Drs expression stained for

1028 activated Dronc (red) via the CC3-antibody, JNK-dependent transcriptional activation via the TREGFP1b reporter

1029 (green) and nuclei size and disintegration via DAPI (white). Arrows in magnified images point towards strong

1030 CC3-staining correlating with disintegrating nuclei. Insets represent DAPI staining and scalebars correspond to

1031 100 μm. (B.) Quantifications of CC3-staining per gland normalized for SG size in Ras^{V12}-glands with in- (Drs) or

1032 decreased (Drs^{RNAi}) Drs expression. Lower/upper hinges of boxplots in (A./C./F.) indicate 1st/3rd quartiles, whisker

1033 lengths equal 1.5*IQR, red circle and bar represent mean and median. Significance evaluated by Student's t-tests

1034 (*** $p<0.001$, ** $p<0.01$, * $p<0.05$, n.s. $p≥0.05$).

1035

Figure 7. Drs inhibits the JNK-feedback loop (A.) Schematic representation of the JNK-feedback loop including levels of interference (blue) and employed read-outs of its activity (green). *hid*-overexpressing glands with or without coexpressed Drs were quantified for (B.) activated basket via a phosphorylation sensitive antibody and (C.) activated Dronc via the CC3-antibody. (D.) Activated basket (pBsk) was quantified and normalized to SG size. (E.) Ras^{V12}-glands with or without Drs-coexpression were stained for activated basket (green) and activated Dronc (red). (F.) Activated basket was detected in Ras^{V12}-glands with or without Dronc-knock-down. Insets: (E./F.) DAPI. Scalebars: (E./F.) 100 μm. Boxplots in (B./C./D.): lower/upper hinges indicate $1^{st}/3^{rd}$ quartiles, whisker lengths equal 1.5*IQR, red circle and bar represent mean and median. Significance evaluated by Student's t-tests (*** $p<0.001$, ** $p<0.01$, * $p<0.05$, n.s. $p≥0.05$).

1046

Supplemental Figure 7. (A.) *Ras^V12*-glands with or without Dronc-knock-down were stained for activated basket with a phosphorylation sensitive antibody at 120 h AED and (B.) the signal was quantified per SG and normalized for its size. Results for both RNAi-lines used, 23035/GD and 100424/KK, were consistent. Insets in (A.) show DAPI and scalebar represents 100 µm. Lower/upper hinges of boxplots in (B.) indicate 1st/3rd quartiles, whisker lengths equal 1.5*IQR, red circle and bar represent mean and median. Significance evaluated by Student's t-tests (*** *p<0.001*, ** *p<0.01*, * *p<0.05, n.s. p≥0.05*).
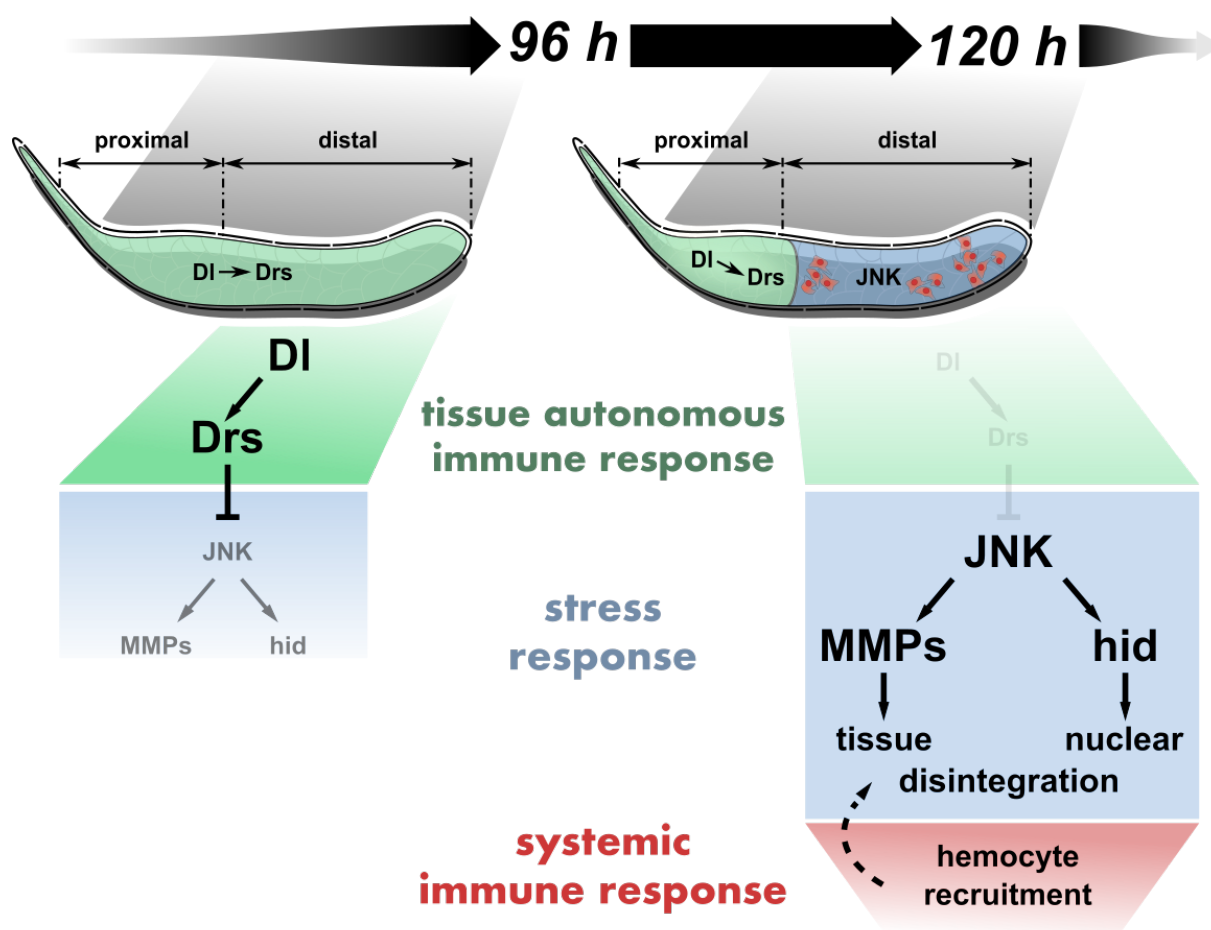
Figure 8. Tissue-autonomous antagonizes systemic immune response via JNK-inhibition in *Ras^V12*-glands
Dorsal-mediated Drs expression inhibits JNK activation in the entire *Ras^V12*-gland until 96 h AED. At 120 h AED, Dorsal and thus Drs expression is reduced to the PP, derepressing full JNK-activation in the DP. Consequently, JNK-dependent expression of hid and MMP2 stimulates nuclear and tissue disintegration, which eventually leads to the interference with tissue growth and integrity by the systemic immune response.